

1 Regime Shifts in Arctic Terrestrial Hydrology  
2 Manifested From Impacts of Climate Warming

3 Michael A. Rawlins<sup>1</sup> and Ambarish V. Karmalkar<sup>2,1</sup>

4 <sup>1</sup>Department of Earth, Geographic, and Climate Sciences, University  
5 of Massachusetts, Amherst, MA 01003, USA

6 <sup>2</sup>Department of Geosciences, University of Rhode Island, Kingston,  
7 RI 02881, USA

8 *Correspondence to:* Michael A. Rawlins (mrawlins@umass.edu)

9 **Abstract**

10 Anthropogenic warming in the Arctic is causing hydrological cycle inten-  
11 sification and permafrost thaw, with implications for flows of water, carbon,  
12 and energy from terrestrial biomes to coastal zones. To better understand  
13 likely impacts of the changes, we used a hydrology model driven by mete-  
14 orological data from atmospheric reanalysis and two global climate models  
15 for the period 1980–2100. The hydrology model accounts for soil freeze-thaw  
16 processes and was applied across the pan-Arctic drainage basin. The simula-  
17 tions point to greater changes over northernmost areas of the basin underlain  
18 by permafrost, and the western Arctic. An acceleration of simulated river  
19 discharge over the recent past is commensurate with trends drawn from ob-  
20 servations and reported in other studies. Between early (2000–2019) and late  
21 century (2080–2099) the model simulations indicate an increase in annual total  
22 runoff of 17–25%, while the proportion of runoff emanating from subsurface  
23 pathways is projected to increase 13–30%, with the largest changes noted in  
24 summer and autumn, and across areas with permafrost. Most notably, runoff  
25 contributions to river discharge shift to northern parts of the Arctic basin that  
26 contain greater amounts of soil carbon. Each season sees an increase in sub-  
27 surface runoff, spring is the only season where surface runoff dominates the  
28 rise in total runoff, and summer experiences a decline in total runoff, despite

29 an increase in the subsurface component. The greater changes that are seen  
30 in areas where permafrost exists supports the notion that increased soil thaw  
31 is shifting hydrological contributions to more subsurface flow. The manifesta-  
32 tions of warming, hydrological cycle intensification, and permafrost thaw will  
33 impact Arctic terrestrial and coastal environments through altered river flows  
34 and the materials they transport.

## 35 **1 Introduction**

36 Hydrological cycle intensification and permafrost thaw are among a myriad of  
37 environmental changes reshaping the Arctic environment (Rawlins et al., 2010; Hinz-  
38 man et al., 2013; Box et al., 2019; Overland et al., 2019). Climate forcings including  
39 increasing air temperature and precipitation are key drivers of alterations to the  
40 Arctic system (Box et al., 2019). The Arctic has warmed 2.5 to 4 times faster  
41 than the global average over the past several decades (Rantanen et al., 2022; Wang  
42 et al., 2022) and experienced substantial decreases in Arctic Ocean sea ice extent  
43 and volume (Stroeve and Notz, 2018; Serreze and Meier, 2019). Warming is lead-  
44 ing to hydrologic intensification that is projected to drive higher precipitation rates  
45 (Bintanja and Selten, 2014; McCrystall et al., 2021), with concomitant rises in river  
46 discharge (Shiklomanov and Shiklomanov, 2003; Dankers and Middelkoop, 2008).  
47 Permafrost thaw has the potential to change how water is stored and moved, and  
48 to mobilize vast stores of organic carbon sequestered in soils (Frey and Smith, 2005;  
49 Koch et al., 2022; Mohammed et al., 2022; Del Vecchio et al., 2024), and rising river  
50 discharge (Peterson et al., 2002; Wagner et al., 2011; Feng et al., 2021) furthermore  
51 imply associated changes in exports of water, energy, carbon, and other constituents  
52 to coastal zones (Tank et al., 2016; Behnke et al., 2021; Zhang et al., 2021). In  
53 light of these alterations, it is important to better understand how climate warming,  
54 hydrological cycle intensification, and permafrost thaw will impact Arctic terrestrial  
55 hydrology and, in turn, exports of freshwater and associated materials through the  
56 Arctic drainage basin and into coastal zones.

57 The seasonal storage of precipitation in the form of snow is a defining element  
58 of Arctic hydrology, contributing to abundant surface water storages and high river  
59 flows following spring melt. The presence of permafrost is another important element  
60 influencing the region’s water cycle. Climate warming is intensifying Earth’s water  
61 cycle, increasing precipitation, evaporation, evapotranspiration (ET), and river dis-  
62 charge globally (Huntington, 2006, 2010), and across Arctic regions (Peterson et al.,  
63 2002; Déry et al., 2009; Rawlins et al., 2010). Intensification or “acceleration” in-  
64 volves the effects of both atmospheric moisture holding capacity and moisture avail-

65 ability. Declining sea ice is making the Arctic Ocean and its surrounding seas a  
66 more available source of moisture, with locally-driven precipitation recycling great-  
67 est in winter across the Beaufort-Chukchi, Laptev, Kara, and East Siberian Seas  
68 (Ford and Frauenfeld, 2022). Increasing late summer precipitation and a shift to-  
69 ward rainfall runoff is occurring across watersheds in northwest Alaska (Arp et al.,  
70 2020; Rawlins, 2021; Arp and Whitman, 2022). Terrestrial hydrology in the Arctic  
71 is also strongly controlled by the presence of permafrost and the seasonal thawing  
72 and freezing of soils (Tananaev et al., 2020). Permafrost underlies approximately  
73 one fifth of the global land area and influences processes involving runoff, aquatic  
74 biogeochemistry (Frey and McClelland, 2009; Spencer et al., 2015; Hu et al., 2023),  
75 and land-atmosphere greenhouse gas exchanges (Christensen et al., 2004; McKenzie  
76 et al., 2021). Permafrost acts as an impermeable hydrological barrier, helping to  
77 maintain high soil suprapermafrost moisture levels while reducing soil water storage  
78 capacity and constraining subsurface flow (Woo et al., 2008; Walvoord and Kurylyk,  
79 2016). The presence or absence of permafrost and variability in precipitation pro-  
80 cesses lead to varying amounts of surface and subsurface runoff contributions to river  
81 discharge and, in turn, land-ocean exports of freshwater and associated materials.  
82 Warming is causing long-term changes in near-surface soil freeze/thaw cycles and  
83 permafrost (Anisimov and Reneva, 2006; Koven et al., 2013; Guo et al., 2018; Peng  
84 et al., 2018; Biskaborn et al., 2019), with implications for permafrost hydrology (Woo  
85 et al., 2008; Liljedahl et al., 2016; Lafrenière and Lamoureux, 2019; Jin et al., 2022).  
86 Subsidence due to thawing soils will likely lead to more runoff, while significantly  
87 accelerating drying of tundra landscapes in a warming climate (Painter et al., 2023).  
88 Studies suggest that permafrost degradation leads to increased moisture transport  
89 from the surface to deeper soils, potentially contributing to increased river baseflows  
90 (Walvoord and Striegl, 2007) and cold season discharge (St. Jacques and Sauchyn,  
91 2009; Shiklomanov et al., 2013; Tananaev et al., 2016; Rawlins et al., 2019; Debolskiy  
92 et al., 2021; Wang et al., 2021; Liu et al., 2022). In northwest Alaska, positive trends  
93 in air temperature and precipitation are greatest in autumn which, together with  
94 permafrost thaw, is likely leading to enhanced subsurface “suprapermafrost” runoff  
95 during that time (Rawlins, 2021).

96 Climate models are essential tools for understanding how manifestations of cli-  
97 mate warming will alter the Arctic’s terrestrial hydrology and riverine land-ocean  
98 fluxes. Model projections point to future precipitation increases over the 21<sup>st</sup> century  
99 through enhanced regional evaporation and poleward moisture transport (Bintanja  
100 et al., 2020), and sea ice declines (Bintanja and Selten, 2014). Models with the  
101 strongest warming response point to decreased snowfall across the high (70–90 °N)  
102 Arctic. The precipitation increases are firmly linked to Arctic warming and sea-ice

103 decline (Bintanja, 2018; Arp et al., 2020), and are likely to increase river discharge  
104 (Peterson et al., 2002; Zhang et al., 2013). Recent coordinated research programs  
105 have produced bias-corrected climate model data for historical and future condi-  
106 tions from consistent protocol frameworks (Warszawski et al., 2014; Lange, 2021).  
107 Simulations of permafrost dynamics and associated soil freeze-thaw processes require  
108 attention to several key processes absent in many land-surface models (Alexeev et al.,  
109 2007; Nicolsky et al., 2007; Lawrence and Slater, 2008). Slater and Lawrence (2013)  
110 concluded that, in general, permafrost is not well represented by the ensemble of  
111 CMIP5 models. Examining permafrost dynamics in global models participating in  
112 the CMIP6, Burke et al. (2020) found that simulation of active-layer thickness (ALT)  
113 and other key features often fell outside the observed range, with errors attributable  
114 to shallow and poorly resolved soil profiles and structural weaknesses in snow physics  
115 and soil hydrology within some of the models.

116 In this study we use simulations with a permafrost hydrology model with sophis-  
117 ticated soil-freeze thaw algorithms that represent an improvement upon traditional  
118 land-surface models to evaluate how climate alterations linked to warming, primar-  
119 ily hydrological cycle intensification and permafrost thaw, will influence Arctic ter-  
120 restrial hydrology and, in turn, land-ocean riverine freshwater and biogeochemical  
121 fluxes. We begin by examining meteorological data from climate models to un-  
122 derstand the atmospheric forcings and their influence on surface hydrology. Model  
123 simulations are validated against select observations for sublimation, ET, ALT, and  
124 river discharge. We then examine changes over the 21<sup>st</sup> century to gain insights into  
125 how hydrological cycle intensification and permafrost thaw will impact key elements  
126 of Arctic terrestrial hydrology controlling river exports, and test the hypothesis that  
127 within the Arctic drainage basin, changes in subsurface runoff are greatest in per-  
128 mafrost areas.

## 129 **2 Methods**

### 130 **2.1 Study area and spatial grid**

131 The pan-Arctic drainage basin used in this study encompasses approximately  
132 22.45 million square kilometers. It has a wide range of land cover types, from grass-  
133 lands in southern Canada and central Eurasia to boreal forests to tundra in far  
134 northern areas. This domain includes basins of rivers draining to the Arctic Ocean,  
135 Hudson Bay, and the Bering Strait, with the large Yukon River draining into the lat-  
136 ter. The region’s four largest rivers—the Ob, Yenesei, Lena, and Mackenzie—flow  
137 primarily in a south-to-north direction, and account for roughly half (49%) of the

138 pan-Arctic basin area. Model forcing data, simulations, and outputs were produced  
139 on the 25×25 km EASE-Grid (Brodzik and Knowles, 2002). The spatial domain  
140 encompassing the terrestrial pan-Arctic as defined in this study has 35,693 grid cells.  
141 Each grid cell has 23 vertical layers extending to 60 m depth in which water and  
142 energy interact with the soil and vegetation. Thus the model is set up and executed  
143 in three dimensions (2 D horizontal and 1 D vertical) like many similar land surface  
144 models often used to quantify terrestrial hydrological fluxes.

## 145 **2.2 Modeling approach**

146 The modeling approach leverages simulations with the Permafrost Water Bal-  
147 ance Model (PWBM v4) to investigate the impacts of warming, hydrological cycle  
148 intensification, and permafrost thaw on terrestrial hydrological fluxes within and  
149 through the pan-Arctic drainage basin. Many of the details of PWBM have been  
150 documented elsewhere, so a general description is provided here with the reader en-  
151 couraged to obtain more detail from the cited literature. The PWBM simulates all  
152 major elements of the water cycle, including transpiration and soil and surface-water  
153 evaporation, snow storage, sublimation (Rawlins et al., 2003, 2013), runoff (Rawlins  
154 et al., 2021), and soil freeze-thaw. Past applications include assessment of causes  
155 behind record Eurasian discharge (Rawlins et al., 2010); estimation of surface water  
156 dynamics (Schroeder et al., 2010); analysis of present and future water budgets (Clil-  
157 verd et al., 2011); quantification of freshwater and dissolved organic carbon fluxes  
158 (Rawlins et al., 2021); investigation of trends in those fluxes to a coastal lagoon  
159 in northwest Alaska (Rawlins, 2021); and exploration of the links between surface  
160 organic soil properties and moisture dynamics across the Alaska North Slope (Yi  
161 et al., 2022). PWBM operates at an implicit daily time step, with meteorological  
162 forcings (air temperature, precipitation, wind speed) typically drawn from reanalysis  
163 data for regional-scale simulations or, when applied to smaller watersheds, meteo-  
164 rological station data. Daily simulated ET depends on atmospheric demand and  
165 surface and soil conditions. In this study we applied the Hamon function to esti-  
166 mate potential evapotranspiration. The model includes a surface water pool that is  
167 typically transient and most often occurs after snowmelt. Runoff is generated when  
168 (i) the amount of available water at the surface exceeds infiltration capacity and  
169 (ii) the amount of water in a soil layer exceeds field capacity, which is a function of  
170 soil texture. The sum of surface and subsurface runoff from one or more soil layers  
171 within a grid cell constitutes daily total runoff. We use the term “subsurface runoff”  
172 for the water flux that has followed subsurface pathways into the stream. Subgrid  
173 fraction of inundated area (lakes and ponds) are parameterized based on observed

174 data (Du et al., 2016), with total runoff across each grid cell calculated as a weighted  
175 total from the inundated and non-inundated areas. We applied a simple river flow  
176 accumulation and linear routing model (Rawlins et al., 2019) to estimate the tim-  
177 ing shift in discharge export at the coast. The snow model simulates the effects of  
178 seasonal changes in snow density and, in turn, snow thermal conductivity (Liston  
179 et al., 2007; Sturm et al., 1995). Soil freeze-thaw process representations include  
180 a multi-layer soil module with algorithms for unfrozen water dynamics and phase  
181 change, as well as specification of the thermal and hydrological properties of organic  
182 soils (Sazonova and Romanovsky, 2003; Nicolsky et al., 2007). The PWBM has a 60  
183 meter soil column, includes parameterizations for thermal and hydraulic properties  
184 of organic soils, and simulates the effect of depth hoar and wind compaction on snow  
185 density. Rawlins et al. (2013) describe the soil freeze-thaw and snow algorithms, and  
186 calibration procedures, which involve factors controlling ET, snow sublimation, and  
187 subsurface runoff that differ between forest and tundra landscapes. In this study  
188 each transient simulation was preceded by a 50-year spinup on year 1980 to stabilize  
189 soil temperature, moisture, and soil dissolved organic carbon (DOC) pools. While  
190 parameterizations for fields such as soil texture and vegetation cover are fundamen-  
191 tal elements of land surface and hydrological model simulations, simulated runoff in  
192 Arctic regions is most sensitive to the time-varying meteorological forcings (Rawlins  
193 et al., 2003).

194 Permafrost extent is based on end of season soil temperatures. If the soil column  
195 down to the maximum 60 meter depth is frozen, beneath a thawed upper zone (i.e.  
196 active layer), the grid cell is deemed to have permafrost that year. Thus permafrost  
197 state is a binary classification. In the case where soil temperatures are well simulated,  
198 one can assume that there is discontinuous permafrost in regions where many grid  
199 cells classified as permafrost interface with many grid cells classified as seasonally  
200 frozen. The impact of subsidence on permafrost thaw is not accounted for in the sim-  
201 ulations, though the effect may be relatively small (Painter et al., 2023), particularly  
202 in areas lacking polygonal tundra. In models operating at continental scales, esti-  
203 mates of permafrost extent across transition zones between continuous permafrost  
204 and the non-permafrost areas are more uncertain due to limitations resolving spatial  
205 variations.

## 206 **2.3 Meteorological forcings**

207 This study focuses on numerical model simulations that were forced with grid-  
208 ded meteorological data (Table 1). We begin by examining simulations forced with  
209 reanalysis data to characterize dynamics over the recent past. Changes over the 21<sup>st</sup>

210 century were assessed using simulations forced with meteorological data from coupled  
 211 climate models, rather than the hydrology (eg. runoff) from them, as outputs from  
 212 individual models can vary widely, and often imply unrealistic long-term systematic  
 213 changes in water storage and level within entire basins (Bring et al., 2015).

Table 1: Simulations conducted in the study, time period for the transient simulation, and origin of forcing data. Each transient simulation was preceded by a 50 year spinup. For the climate model forcing, the 1980–2100 period includes two different experiments.

<b>Model simulations</b>		
<b>Name</b>	<b>Period</b>	<b>Forcing</b>
PWBM-W5E5	1980–2019	Bias-adjusted ECMWF Reanalysis v5 (ERA5)
PWBM-ERA5	1980–2019	ERA5 Reanalysis
PWBM-MERRA	1980–2013	Modern-Era Retrospective Analysis for Research and Applications
PWBM-IPSL	1980–2100	IPSL-CM6A-LR (Historical: 1980–2014, SSP3-7.0: 2015–2100)
PWBM-MPI	1980–2100	MPI-ESM1-2-HR (Historical: 1980–2014, SSP3-7.0: 2015–2100)

214 Simulations were made using forcings from three reanalysis datasets (W5E5,  
215 ERA5, MERRA) and two global climate models from the Coupled Model Inter-  
216 comparison Project Phase 6 (CMIP6). The WFDE5 data—WATCH Forcing Data  
217 methodology applied to ERA5 reanalysis—is bias-adjusted ERA5 data at  $0.5^\circ \times 0.5^\circ$   
218 spatial and sub-daily resolutions, generated specifically to be used as climate data in-  
219 puts for impacts studies (Cucchi et al., 2020). The WFDE5 over land is merged with  
220 ERA5 over the ocean to produce W5E5 data (Lange, 2019), compiled as part of phase  
221 3b of the Inter-Sectoral Impact Model Intercomparison Project (ISIMIP3b) (Lange,  
222 2019, 2021). We downloaded and analyzed W5E5 version 2 data for use as meteorolo-  
223 gical forcings for simulations over the historical period. We use bias-adjusted data  
224 (W5E5 v2 and climate models) prepared as part of the ISIMIP framework (Cucchi  
225 et al., 2020; Lange et al., 2021). We also applied data from ERA5 and MERRA  
226 reanalysis to gauge the accuracy of the air temperature (2 m), precipitation, and  
227 wind speed forcings and for model validation. Precipitation amounts in the W5E5  
228 data are lowest among the three reanalysis datasets. To ameliorate this bias in the  
229 simulation forced with W5E5 we increased each precipitation value by 20%. The  
230 ISIMIP3b climate model forcing data are bias adjusted and statistically downscaled,  
231 and available for five CMIP6 models (GFDL-ESM4, IPSL-CM6A-LR, MPI-ESM1-  
232 2-HR, MRI-ESM2-0, UKESM1-0-LL) forced with three Shared Socioeconomic Path-  
233 ways (SSP) scenarios (SSP1-2.6, SSP3-7.0, SSP5-8.5). In our two simulations over  
234 years 1980–2100 we used data from two models (MPI-ESM1-2-HR, IPSL-CM6A-LR)  
235 forced with SSP3-7.0, which is a high emissions “business as usual” scenario, and  
236 suitable to investigate the response of Arctic hydrology to a strong climate forcing.  
237 These two climate models generally bracket the range of climate projections for the  
238 pan-Arctic region across the five CMIP6 models (Fig. S1). The selection of these two  
239 models—hereafter IPSL and MPI—is aimed at capturing a wide range of tempera-  
240 ture and precipitation projections, but not necessarily the full range. Air temperature  
241 and precipitation changes expressed by the models are described in Sect. 4.1 and 4.2  
242 respectively. In a study examining which CMIP3 models performed best at capturing  
243 meteorological quantities across parts of the Arctic, a predecessor of the MPI-ESM  
244 ranked highest (Walsh et al., 2008).

## 245 **2.4 Statistical analysis**

246 Our analysis of changes closely connected to Arctic rivers centers on differences  
247 between 20-yr intervals representing early (2000–2019) and late (2080–2099) century  
248 conditions. Specifically we mapped climatological averages over these periods and  
249 examined the differences for each domain grid cell. Domain-wide averages were com-



250 puted from all 35,693 grid cells covering the domain. The statistical significance  
251 of differences between the two periods were calculated for select quantities. Before  
252 applying the statistical significance test we used graphical analysis and the Shapiro–  
253 Wilk test (Shapiro and Wilk, 1965) to determine if the data series of interest is  
254 approximately normally distributed. The paired t test was then applied to test the  
255 null hypothesis that the mean difference between two variables is zero. Relative (per-  
256 centage) difference is calculated based on the standard formula: Relative difference  
257 (%) =  $(Z_2 - Z_1) / Z_1 \times 100$ , where  $Z_1$  and  $Z_2$  are values for early and late periods  
258 respectively.

259 Metrics which rely on squared differences are known to be problematic (Willmott  
260 and Matsuura, 2005; Hodson, 2022). The RMSE in particular is inappropriate be-  
261 cause it is a function of three characteristics of a set of errors, rather than of one  
262 (the average error). RMSE varies with the variability within the distribution of er-  
263 ror magnitudes and with the square root of the number of errors, as well as with  
264 the average-error magnitude (MAE). Interpretation problems can thus arise because  
265 sums-of-squares-based statistics do not satisfy the triangle inequality (Willmott and  
266 Matsuura, 2009). Thus MAE and mean bias error (MBE) are more natural measures  
267 of average error, and evaluations and inter-comparisons in this study are based upon  
268 it.

269 In this study we leverage the simulations forced by the two climate models to  
270 investigate the sensitivity of thermal and hydrological responses to different climate  
271 forcings, not to provide robust quantitative projections, which would require a multi-  
272 model, multi-scenario ensemble.

### 273 **3 Model Validation**

274 We first compared key components of the simulated water budget–active-layer  
275 thickness, sublimation, evapotranspiration, and discharge–with different observa-  
276 tional datasets to assess the credibility of the PWBM simulations. Simulated active-  
277 layer thickness (ALT) and model-estimated permafrost extent is compared to ALT  
278 data from the National Tibetan Plateau/Third Pole Environment Data Center (TPDC)  
279 (Fig. 1a–d) and permafrost area from International Association of Permafrost (IPA)  
280 data. In this study the active layer is the top layer of ground subject to annual  
281 thawing and freezing in areas underlain by permafrost. Simulated ALT in the model  
282 simulations spans a greater range compared with the TPDC data (Fig. 1e). However,  
283 the TPDC ALT estimates are known to have a reduced distribution range owing to  
284 the machine learning approach used (Ni et al., 2021). As Ran et al. (2022) described  
285 in their analysis of the TPDC dataset, the uncertainty of ALT is considerable, espe-

286 cially in the vast area of western Siberia where the training data are sparse. Further,  
287 they suggested that the low spatial representativeness of training data may have led  
288 to an overestimation in several Siberian mountain regions and underestimation near  
289 the lower boundary of permafrost. Moreover, in situ ALT is obtained at a point  
290 location that may not be representative of the region in which it is located. In light  
291 of these uncertainties, permafrost extent is generally well captured, with differences  
292 from total area of continuous and discontinuous permafrost in the IPA dataset of  
293 less than 10% (Table 2). For comparison, the fraction of continuous, discontinuous,  
294 and sporadic/isolated permafrost within the major river basins is shown in Table 3.  
295 In Eurasia there exists a clear west-east gradient, with the relatively cold Lena basin  
296 having a large amount of continuous permafrost. In North America the Mackenzie  
297 basin has a large extent of land in the south devoid of permafrost, a reflection of the  
298 relatively warm climate there.

299 We used the simulation forced with W5E5 data (PWBM-W5E5) to evaluate the  
300 magnitude of vertical fluxes of water from sublimation and ET over the recent past  
301 (Fig. 2). Overestimates in simulated sublimation (Figure S2a) are noted (domain-  
302 wide average sublimation of  $40 \text{ mm yr}^{-1}$  for GLEAM and  $57 \text{ mm yr}^{-1}$  for PWBM-  
303 W5E5), though the discrepancy is small relative to the magnitudes of annual total  
304 runoff and ET (MAE =  $27 \text{ mm yr}^{-1}$ ). Simulated ET ( $260 \text{ mm yr}^{-1}$ ) generally  
305 falls between the estimates from GLEAM ( $304 \text{ mm yr}^{-1}$ ) and remote sensing-based  
306 data ( $230 \text{ mm yr}^{-1}$ ), differences of 14% and 12% (MAE of 64 and  $198 \text{ mm yr}^{-1}$ )  
307 respectively. The model generally captures the spatial pattern in sublimation and  
308 ET, though regionally there are notable differences, particularly across the warmer  
309 southerly areas where PWBM tends to underestimate ET (Figure S2b,c). For runoff  
310 this result points to a possible wet bias in those areas relative to observed conditions.

311 We compared simulated discharge volume to a new dataset, the Remotely-sensed  
312 Arctic Discharge Reanalysis (RADR), that was generated through assimilation of ap-  
313 proximately 9.18 million discharge observations derived from 227 million river width  
314 measurements from Landsat images (Feng et al., 2021). Simulated discharge vol-  
315 ume is the sum total of runoff over the contributing river basin. This evaluation  
316 was performed for total discharge from the pan-Arctic drainage basin and five large  
317 Arctic rivers: the Ob, Yenesei, Lena, Mackenzie, and Yukon (Fig. S3). The model  
318 tends to overestimate discharge across western Eurasia and underestimate it across  
319 eastern Eurasia. Differences are modest for the two North American rivers. Yet the  
320 magnitude of pan-Arctic discharge is well constrained. Average freshwater export  
321 to the Arctic Ocean from the study domain over the period 1984–2018 is  $5,169 \text{ km}^3$   
322  $\text{yr}^{-1}$  based on RADR. Over the same period, annual total discharge is 5752, 5822,

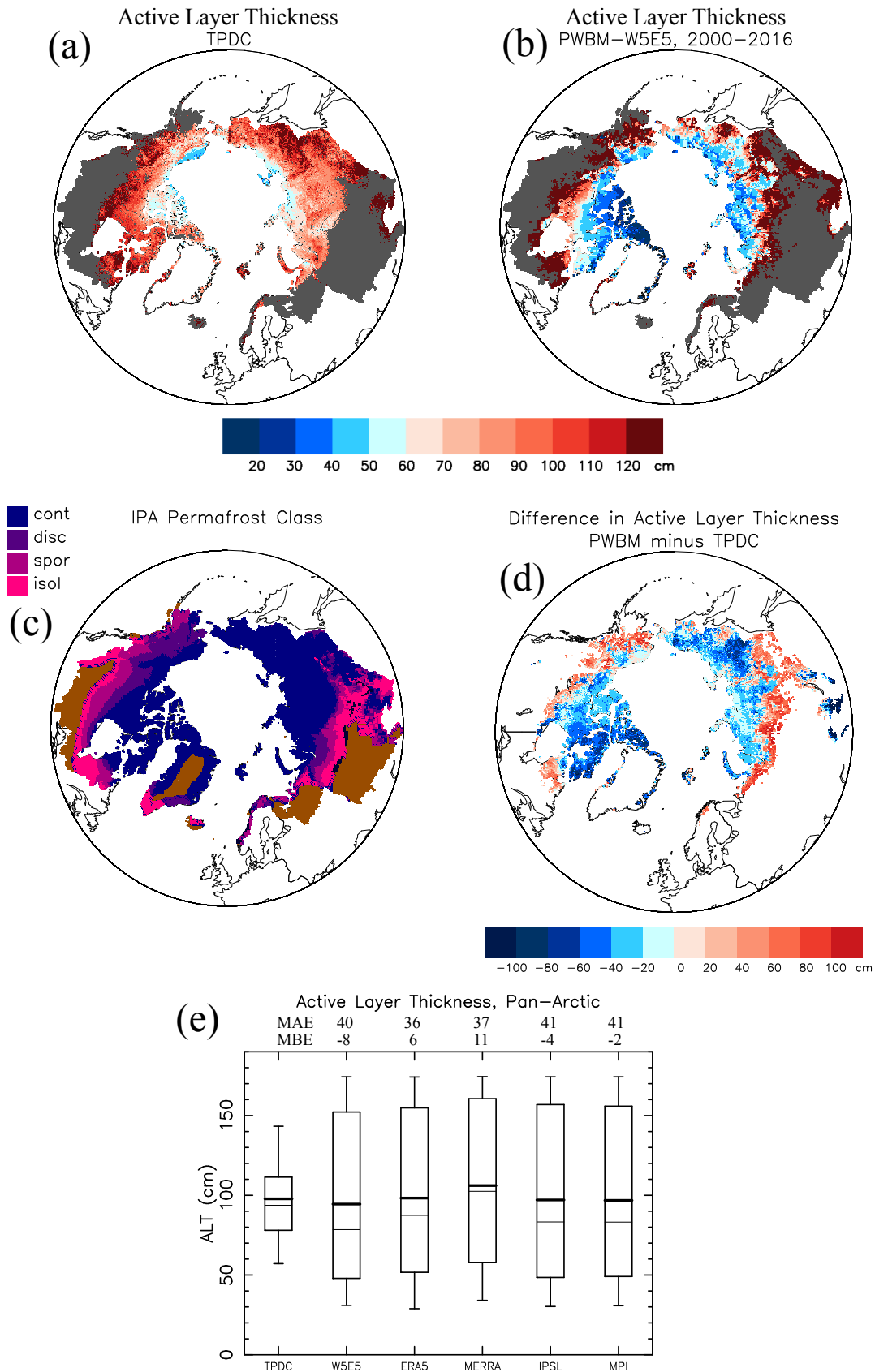


Figure 1: (a) Active-layer thickness (ALT, cm) from the TPDC database (Ran et al., 2022) for the period 2000–2016, and (b) from the PWBM simulation forced with W5E5 data over same period. Grey shading indicates non-permafrost areas. (c) Permafrost classification from International Association of Permafrost (IPA) data. (d) Difference in ALT (cm) between PWBM and TPDC. (e) Distributions of annual maximum ALT (cm) for all grids with permafrost. ALT is the average for each year over the period 2000–2016. TPDC is used as validation for the ALT estimated by simulations forced with data from W5E5, ERA5, MERRA (2000–2013), IPSL, and MPI. Boxplot rectangles bracket the 25<sup>th</sup> and 75<sup>th</sup> percentiles. Whiskers extend to the 5<sup>th</sup> and 95<sup>th</sup> percentiles. Thick and thin horizontal lines mark the distribution mean and median respectively. Mean absolute error (cm) and mean bias error (cm) shown.

Table 2: Permafrost areal extent and difference from observed extent across the study domain. Area in million km<sup>2</sup> from the International Permafrost Association (IPA) classification (Brown et al., 2001), the National Tibetan Plateau Data Center (TPDC) dataset (Ran et al., 2022), and PWBM simulations. Areas of continuous and discontinuous permafrost were added for the IPA estimate. Difference is defined based on observations from the IPA-based extent. For the simulated estimates, a grid cell is deemed to have permafrost under the standard definition of ground (model soil layer) that remains at or below 0°C for at least 2 consecutive years.

<b>Data</b>	<b>Area (10<sup>6</sup> km<sup>2</sup>)</b>	<b>Difference (%)</b>
IPA	13.2	–
TPDC	12.5	–5.5
PWBM-W5E5	12.7	–4.2
PWBM-ERA5	13.1	–0.8
PWBM-MERRA	10.5	–20.4
PWBM-IPSL	12.4	–6.2
PWBM-MPI	11.8	–10.9

Table 3: Permafrost coverage by class in percent (%) for major river basins of the terrestrial Pan-Arctic. The fraction of land without permafrost is in column non-PF.

<b>Basin</b>	<b>continuous</b>	<b>discontinuous</b>	<b>sporadic/isolated</b>	<b>non-PF</b>
Ob	4.3	3.8	5.0	86.9
Yenesei	31.9	11.0	51.9	5.2
Lena	77.4	12.9	9.4	0.3
Mackenzie	15.7	29.6	47.3	7.4
Yukon	18.8	68.1	13.1	0.0

323 and 5811 km<sup>3</sup> yr<sup>-1</sup> in the simulations forced by W5E5, IPSL, and MPI respectively  
324 (Fig. S4), giving differences from RADR discharge of less than 13%. The simulation  
325 forced with W5E5 captures the acceleration in Arctic discharge reported in other  
326 studies (Peterson et al., 2002; Feng et al., 2021). The linear trend of 8.3 km<sup>3</sup> yr<sup>-2</sup>  
327 (0.15% yr<sup>-1</sup>) closely aligns with the acceleration (11.6 km<sup>3</sup> yr<sup>-2</sup>, 0.22% yr<sup>-1</sup>) from  
328 RADR discharge (Feng et al., 2021), and is in the upper range of estimates (3.5–  
329 10 km<sup>3</sup> yr<sup>-2</sup>) from prior studies (Shiklomanov et al., 2000; McClelland et al., 2006;  
330 Rawlins et al., 2010). For comparison, an analysis for the four largest Arctic-draining  
331 rivers (Mackenzie, Ob, Yenisei, and Lena) indicates that the combined annual dis-  
332 charge increased by 89 km<sup>3</sup> decade<sup>-1</sup> over the period 1980–2009, amounting to an  
333 approximate 14% increase over the 30-year period (Ahmed et al., 2020). Hydrologi-  
334 cal cycle intensification is connected with warming, and also manifested by increases

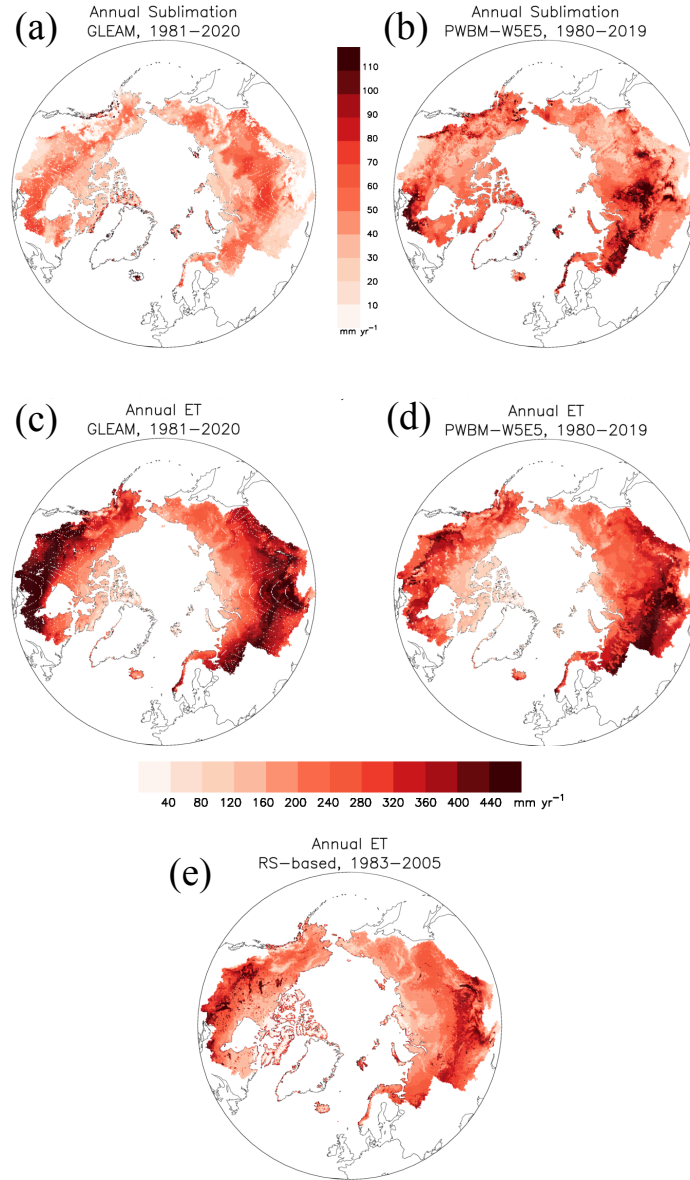


Figure 2: (a) Annual total sublimation ( $\text{mm yr}^{-1}$ ) and (c) evapotranspiration (ET,  $\text{mm yr}^{-1}$ ) from GLEAM (Miralles et al., 2011; Martens et al., 2017) and PWBM-W5E5 (b,d). Bottom panel (e) shows ET from a dataset derived from remote sensing data (Zhang et al., 2009).

335 in vertical fluxes of precipitation and ET. The differences of less than 15% between  
 336 model simulated ET and discharge, and the estimates from the validation datasets,

337 suggests that the water budget components are sufficiently well constrained to enable  
 338 evaluation of the impact of climate warming on runoff and river discharge in Arctic  
 339 rivers. In general, the comparisons with observations support the model’s ability to  
 340 reliably simulate key hydrological variables of interest.

## 341 4 Alterations connected to hydrological cycle in- 342 tensification and permafrost thaw

### 343 4.1 Air temperature

344 In this analysis we use the simulations forced by the two climate models to bracket  
 345 changes likely to occur this century, focusing primarily on twenty-year periods repre-  
 346 senting early (2000–2019) and late (2080–2099) century conditions. The IPSL model  
 347 projects stronger warming compared to MPI, with warming between early and late  
 348 century of 7.2 °C (domain-wide mean value) and 6.2 °C, respectively (Table 4). Both  
 349 show the strongest warming over the highest latitudes of the pan-Arctic basin, with  
 350 warming of over 10 °C across far northern Canada projected by IPSL. More modest  
 351 warming of 3–4 °C is noted over southwestern Canada and central Eurasia in the  
 MPI data.

Table 4: Climatological averages for early (2000–2019) and late (2080–2099) century periods from the simulations forced with IPSL and MPI meteorological data. <sup>a</sup>Relative (percentage) difference shown for each except air temperature, which is shown in degrees C. Differences are statistically significant for all quantities listed based on the paired T test (Sect. 2.4).

Variable	PWBM-IPSL			PWBM-MPI		
	early	late	% diff <sup>a</sup>	early	late	% diff <sup>a</sup>
air temp (C)	−5.3	1.9	7.2	−5.3	−0.9	6.2
precipitation (mm yr <sup>−1</sup> )	578	697	21	573	643	12
net precipitation (mm yr <sup>−1</sup> )	258	315	22	259	300	16
rainfall (mm yr <sup>−1</sup> )	334	437	31	354	413	17
snowfall (mm yr <sup>−1</sup> )	244	260	7	219	230	5
rainfall fraction (%)	56	62	11	43	63	47
runoff (mm yr <sup>−1</sup> )	264	329	25	266	310	17
F <sub>sub</sub> (%)	27	35	30	30	34	13

352

353 In the results that follow, unless otherwise noted, statements reporting two statis-  
354 tics will be written in order for PWBM-MPI and PWBM-IPSL respectively. In nearly  
355 every instance, changes are greater with the latter simulation due to the influence of  
356 forcing from the more strongly warming (and wetter) IPSL climate model.

## 357 4.2 Precipitation

358 Rainfall rates have also been increasing across much of the pan-Arctic. Rainfall  
359 will continue to increase this century, particularly along favored storm track regions  
360 over northwestern Eurasia and western Alaska (Fig. 3a, S5a), where the majority of  
361 water vapor transport into the Arctic occurs (Nash et al., 2018). Climatological aver-  
362 age rainfall (domain average) is higher by late century, with relative differences of 17  
363 and 31% for the MPI and IPSL models, respectively (Table 4). Snowfall is projected  
364 to increase over a smaller geographic extent, mainly the higher latitudes and across  
365 the colder parts of eastern Eurasia, and decrease over most of the pan-Arctic, most  
366 prominently western Eurasia and southern Canada (Fig. 3b, S5b). The domain-wide  
367 change averages 5 and 7%. The sizable rainfall increases drive the projected rise in  
368 the fraction of rainfall to total precipitation (Fig. 3c, S5c) averaging 11 and 47%  
369 for the two simulations. Net precipitation—the difference between precipitation and  
370 the sum of evapotranspiration and snow sublimation—is projected to increase across  
371 most ( $> 75\%$ ) of the pan-Arctic basin. Decreases will occur across southern Canada  
372 and Eurasia. For areas with and without permafrost, mean changes (increases) are 31  
373 and 42%, and 5 and 6%, respectively. The simulations thus reveal bigger impacts—a  
374 net wetting—over permafrost regions, and a strong latitudinal south-north gradi-  
375 ent in future precipitation changes that will influence river discharge quantity and  
376 quality.

## 377 4.3 Permafrost extent and active layer thickness

378 Research studies have documented hydrological cycle intensification and per-  
379 mafrost thaw across the terrestrial Arctic. To better understand changes in per-  
380 mafrost hydrology attributable to warming and increasing soil thaw we calculated  
381 ALT averages from the two climate-model-forced simulations (Fig. 4, S6). For  
382 PWBM-IPSL, permafrost area decreases by 7.8 million  $\text{km}^2$  (12.3 to 4.5 million  $\text{km}^2$ )  
383 from the early to late century periods, a decline of 63% of present day permafrost  
384 area. For PWBM-MPI, some 4.9 million  $\text{km}^2$  or 42% of present area loses permafrost  
385 (11.7 to 6.8 million  $\text{km}^2$ ). Predictions of soil temperature from CMIP5 models point  
386 to permafrost fractional losses by end of century of 15% to 87% for RCP4.5, and 30%

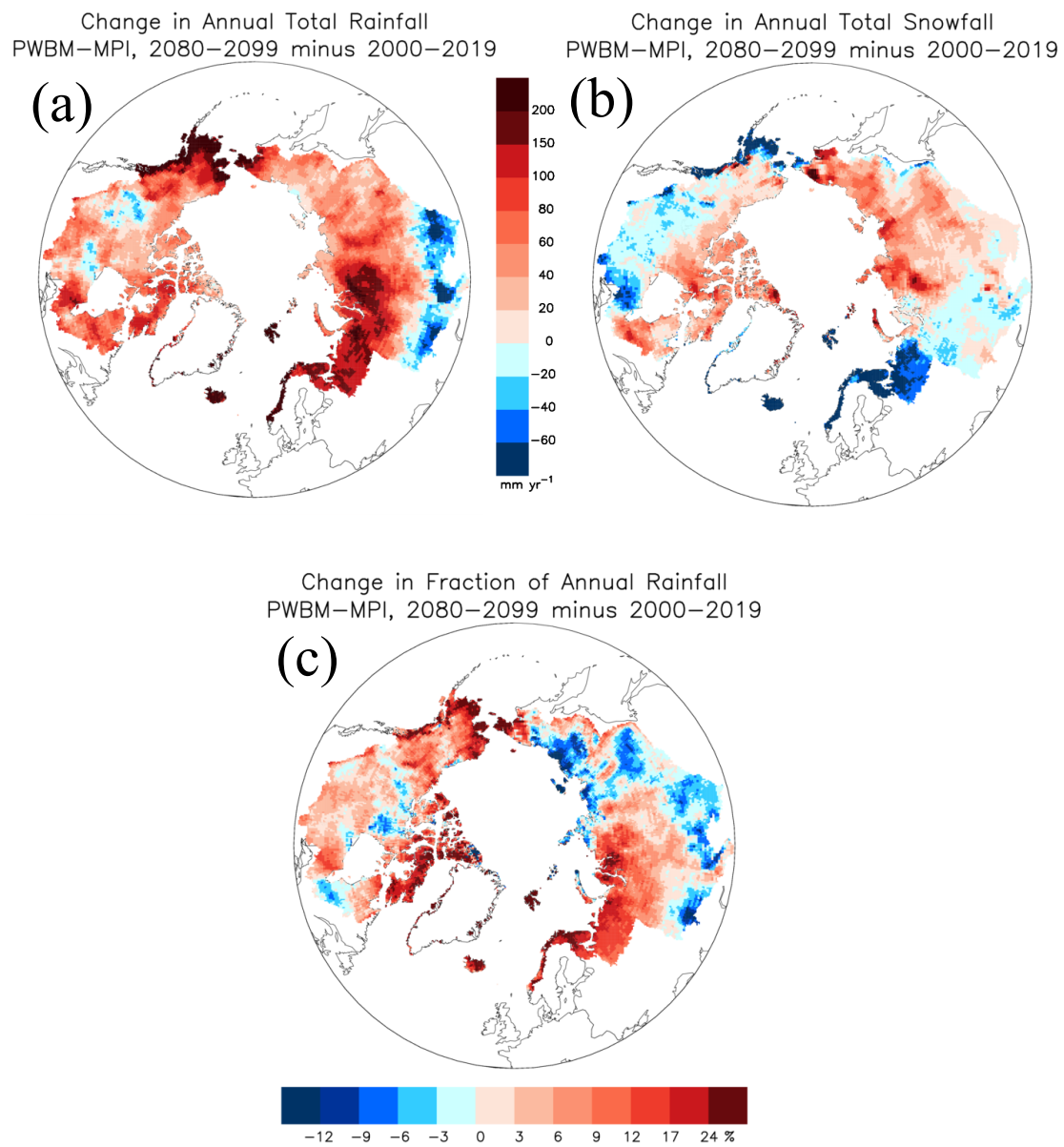


Figure 3: Change in (a) annual rainfall (mm yr<sup>-1</sup>), (b) snowfall (mm yr<sup>-1</sup>), and (c) the fraction of rainfall to total precipitation from PWBM-MPI simulation.



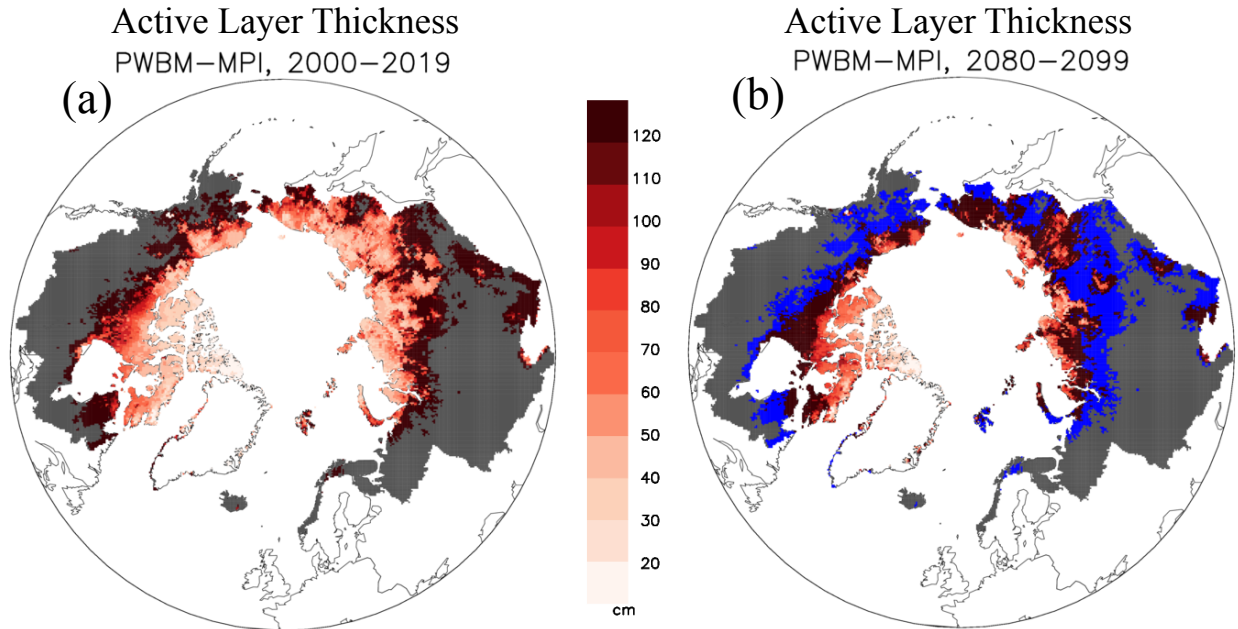


Figure 4: Simulated active-layer thickness (ALT, cm) for (a) early (2000–2019) and (b) late century (2080–2099) periods from PWBM-MPI. Blue shading highlights areas that are no longer characterized as permafrost in the future period. Gray areas are non-permafrost areas of the Arctic basin.

387 to 99% for RCP8.5 (Koven et al., 2013). Across areas that maintain permafrost, the  
 388 ALT increases between the two periods average 56 and 91 cm. For comparison, esti-  
 389 mates over permafrost areas obtained from an air temperature-based thawing index  
 390 applied to 16 CMIP5 models (2006–2100) forced under RCP8.5 averaged a similar  
 391  $6.5 \text{ cm decade}^{-1}$ .

#### 392 4.4 Runoff and river discharge

393 Annual runoff within the pan-Arctic basin is typically highest across eastern  
 394 Canada, western Eurasia, and coastal regions of western Canada and western Alaska.  
 395 Runoff changes between the early and late century periods were calculated here to  
 396 assess future alterations to river discharge (Fig. 5a, S7a). In Eurasia the change in  
 397 annual total runoff, as a percent of the early period, is greater over northeast parts  
 398 of the continent. Across North America the increases are also greater in the colder  
 399 northern parts of the Canadian archipelago and over northern Alaska. Averaged  
 400 across all grid cells, annual runoff increases by 19% ( $45 \text{ mm yr}^{-1}$ ) and 31% ( $65 \text{ mm}$   
 401  $\text{yr}^{-1}$ ) from PWBM-MPI and PWBM-IPSL, respectively. Not surprisingly, the spatial  
 402 pattern in runoff change closely aligns with the pattern in net precipitation. There  
 403 is also a significant difference in the mean change in annual runoff between grid cells  
 404 with permafrost (67 and  $99 \text{ mm yr}^{-1}$  increase) and those without permafrost (21 and  
 405  $25 \text{ mm yr}^{-1}$ ). This divergence is driven by changes in net precipitation (64 and 89

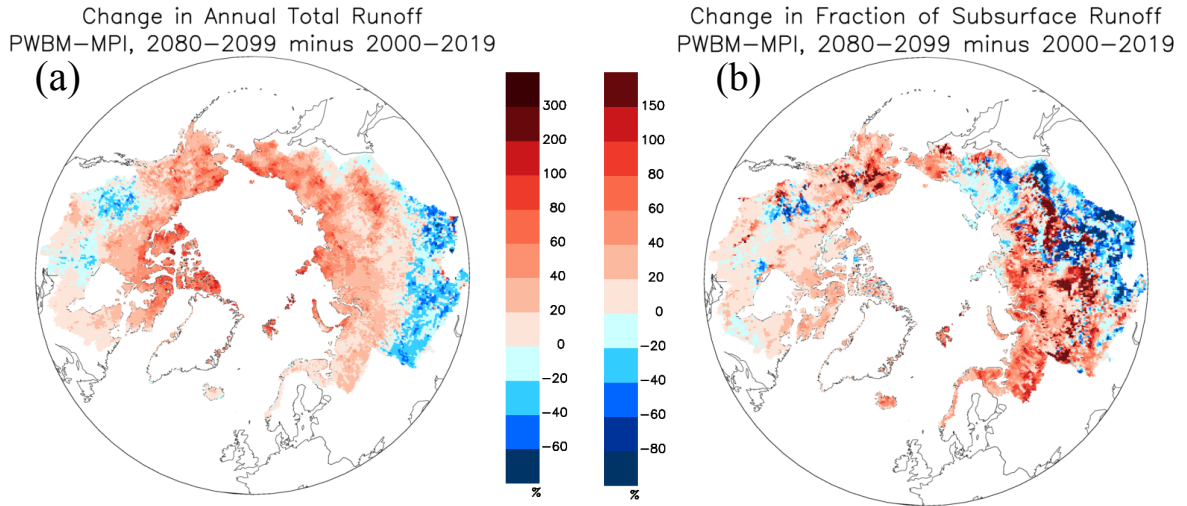


Figure 5: Change in (a) annual total runoff (%) and (b) fraction of subsurface to total runoff ( $F_{sub}$ , %) from the simulations.

406 mm yr<sup>-1</sup> vs. 18 and 19 mm yr<sup>-1</sup>), as well as differing influences from deepening ALT  
 407 and longer thawed periods in areas with and without permafrost. Across permafrost  
 408 areas, the difference between net precipitation and runoff—in a water budget, an  
 409 approximation for change in storage—is 3–10 mm yr<sup>-1</sup>, a small amount relative to  
 410 the runoff increase. Over the early century period, river discharge volume is 5839,  
 411 5955, 5917 km<sup>3</sup> yr<sup>-1</sup> for the PWBM-W5E5, PWBM-MPI, PWBM-IPSL simulations  
 412 respectively (Fig. S4). By late century, discharge volume increases to 6955 and  
 413 7374 km<sup>3</sup> yr<sup>-1</sup>, relative increases of 17 and 25% for PWBM-MPI, and PWBM-IPSL  
 414 respectively (runoff equivalents in Table 4). The trend is statistically significant ( $p$   
 415  $< 0.01$ ) for both time series.

416 A transition from runoff dominated by surface water contributions toward in-  
 417 creasing amounts of subsurface flow is expected as the climate warms (Frey and  
 418 McClelland, 2009). Compared to change in total runoff, the change in the fraction  
 419 of subsurface to total runoff ( $F_{sub}$ ) is more spatially variable across the pan-Arctic  
 420 (Fig. 5b, S7b). During the early century period,  $F_{sub}$  averages 30% and 27% in the  
 421 PWBM-MPI and PWBM-IPSL simulations respectively (Fig. 6). The fractions in-  
 422 crease to 34% and 35% by end of century, giving relative (percent) increase in domain  
 423 mean  $F_{sub}$  of 13 and 30% for PWBM-MPI and PWBM-IPSL respectively. Based on  
 424 the modest warming PWBM-MPI run, approximately 72% of permafrost areas will

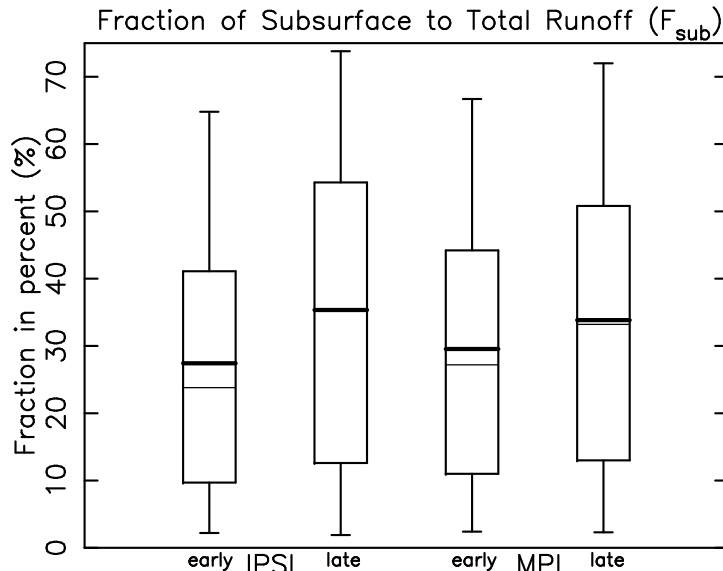


Figure 6: Fraction of subsurface to total runoff ( $F_{sub}$ ) for early and late century periods for all pan-Arctic grids from PWBM-IPSL and PWBM-MPI simulations.

425 have higher subsurface runoff fractions by end of century. This spatial extent in-  
 426 creases to 88% of the permafrost region under the more aggressive warming depicted  
 427 under PWBM-IPSL (Fig. S7b). The shift in  $F_{sub}$  is larger in permafrost areas, with  
 428 significant differences in spatial mean  $F_{sub}$  in areas with and without permafrost  
 429 (relative differences 15.7 and 13.5% respectively for PWBM-MPI; 31.1 and 24.4%  
 430 for PWBM-IPSL). The PWBM-MPI simulation reveals a significant relationship ( $p$   
 431  $< 0.01$ ) between change in ALT and  $F_{sub}$ , with a 6.4% increase in  $F_{sub}$  per 0.1 m  
 432 increase in ALT. While the positive correlation does not exist under PWBM-IPSL,  
 433 the more pervasive growth in  $F_{sub}$  in PWBM-MPI suggests a connection between soil  
 434 thaw and increasing contributions from subsurface runoff to river discharge during  
 435 this century, particularly in regions underlain by permafrost.

436 The runoff changes in both simulations exhibit a significant positive relationship  
 437 with latitude (Fig. 7a, S8a). The linear fit suggests an additional 2.9 and 4.2% runoff  
 438 (PWBM-MPI and PWBM-IPSL) for each degree northward in latitude. Under this  
 439 pattern river discharge shifts over time to being sourced more from the northerly  
 440 parts of the four largest river basins (Ob, Yenesev, Lena, Mackenzie; Fig. 8a, S9a,  
 441 Table 5). Decreases are projected for the southerly half of the Ob, Yenesev, and  
 442 Mackenzie Rivers. For the Ob basin, less runoff across the southern half of the river  
 443 basin will be offset by higher flow in the north, so that annual total discharge exported

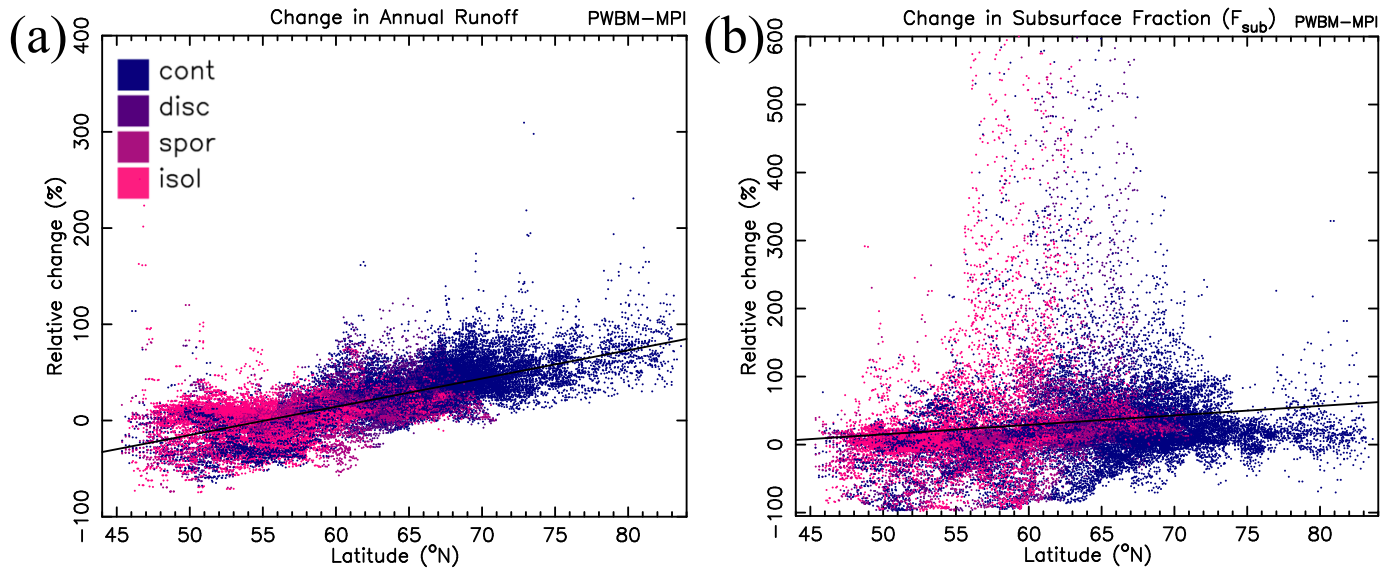


Figure 7: Change in (a) annual total runoff (%) and (b)  $F_{sub}$  with grid cell latitude from PWBM-MPI simulation for all pan-Arctic domain grid cells. Colors indicate permafrost classification (continuous, discontinuous, sporadic, or isolated) for the cell from IPA dataset (Figure 1c).

444 at the coast is relatively unchanged. The Yeneseý shows a similar pattern, with  
 445 accumulated discharge at the coast higher by late century. The Lena and Mackenzie  
 446 Rivers will receive substantial additional discharge from their northern areas, with  
 447 the Lena projected to export 66 and 128 km<sup>3</sup> yr<sup>-1</sup> (16 and 31%) more freshwater  
 448 discharge by late century. The sharp increase in export from the Yeneseý and Lena  
 449 arising from their northern watersheds is driven primarily by higher snowfall rates  
 450 (Fig. 3b, S5b). Averaged across the four, the downstream half of the rivers will  
 451 receive approximately 20–30% more accumulated discharge from the northern half  
 452 of their contributing area. A south-north gradient also exists in soil carbon storage  
 453 in these basins, with the highest amounts in the far north (Fig. 8b, S9b). Subsurface  
 454 runoff increases are also greater to the north (Fig. 7b, S8b), though the scatter is  
 455 substantial compared to the change in annual total runoff.

456 Runoff is projected to increase during most months in both simulations (Fig. 9, S10),  
 457 with monthly changes remarkably similar between the two runs. Averaged over sea-  
 458 sons, runoff increases (depth in mm) are greatest in spring (MAM). The increase in  
 459 spring, particularly during May, is attributable to additional snowmelt runoff and  
 460 a shift to earlier snowpack melting. As a consequence, less snowmelt and runoff  
 461 occur in June. Averaged across the six largest rivers (Ob, Yeneseý, Lena, Mackenzie,  
 462 Yukon, Kolyma), peak daily discharge at each coastal outlet shifts earlier by end of

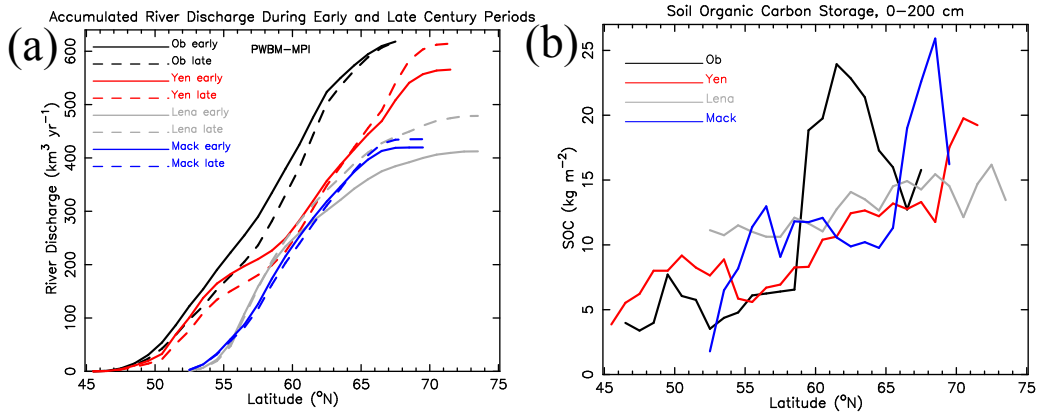


Figure 8: (a) Accumulated annual total river discharge ( $\text{km}^3 \text{ yr}^{-1}$ ) for the Ob, Yeneseey, Lena, and Mackenzie Rivers for  $1^\circ$  latitude bands as averages over early (solid line) and late (dashed) century periods from PWBM-MPI. (b) Soil carbon storage ( $\text{kg m}^{-2}$ ) in soil 0–200 cm zone from the Northern Circumpolar Soil Carbon Database (Hugelius et al., 2013).

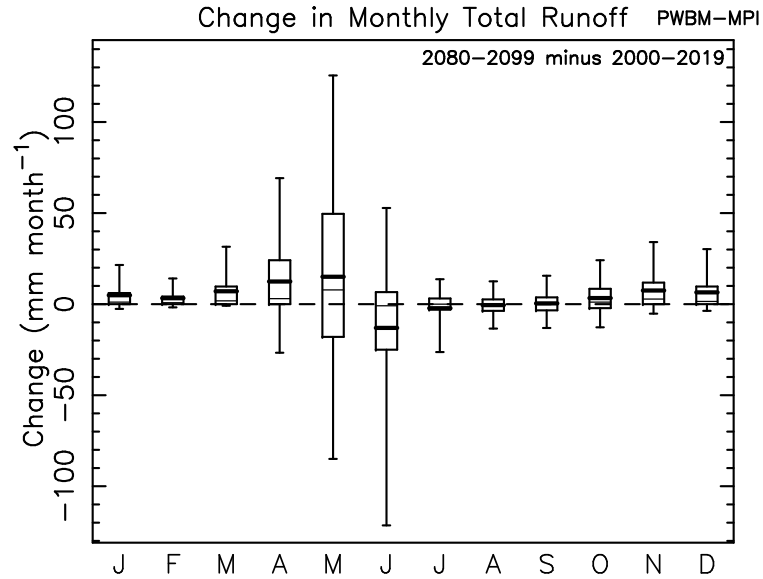


Figure 9: Distribution in change in monthly total runoff ( $\text{mm month}^{-1}$ ) between early and late century periods for all pan-Arctic grid cells from PWBM-MPI.

Table 5: Relative (percentage) change in accumulated river discharge for the upstream (southern) half and downstream (northern) half of each of the four largest Arctic rivers. Averages are calculated from the totals shown in Fig.s 8, S7. Total row represents the average from the four.

River	PWBM-IPSL		PWBM-MPI	
	up (%)	down (%)	up (%)	down (%)
Ob	-9.8	7.4	-19.4	13.6
Yenesey	-1.5	27.9	-14.2	22.2
Lena	26.4	43.8	12.5	25.9
Mackenzie	-0.2	35.3	-5.3	17.3
Total	3.7	28.6	-6.6	19.7

463 century by approximately 11 days in both simulations (DOY 180 to 169 in PWBM-  
 464 IPSL and DOY 176 to 165 in PWBM-MPI). Runoff is largely unchanged in July,  
 465 August and September, and the changes are not statistically significant in June and  
 466 July due to the high degree of spatial variability. Seasonally, the relative change  
 467 (percentage change) is greatest in winter, with runoff by late century a factor of  
 468 5–10 greater compared to the early century period averages. Significant percentage  
 469 increases are noted in autumn and spring as well. Interestingly, snow storage (snow  
 470 water equivalent, SWE) increases in both simulations are significant in February,  
 471 March, and April only. Notably, no increase in SWE is projected during autumn.

472 The intensifying hydrological cycle and thawing permafrost will manifest in chang-  
 473 ing amounts of surface and subsurface runoff contributions to river discharge (Fig. 10).  
 474 The shifts vary strongly with season, and spatially across the terrestrial Arctic, with  
 475 remarkably similar change magnitudes in the two simulations, due largely to similar-  
 476 ities in patterns in net precipitation and its change this century. At the pan-Arctic  
 477 scale, modest increases are projected in both surface and subsurface runoff for the  
 478 annual total and in winter, spring, and autumn. The acceleration during winter and  
 479 autumn will come predominantly from additional subsurface runoff. Spring increases  
 480 are mainly attributable to increased surface runoff. Runoff is projected to decrease  
 481 slightly in summer due to less surface runoff, despite a small increase in subsur-  
 482 face runoff. The autumn change is particularly noteworthy over northern Alaska.  
 483 Also there, summer shows a strong shift from surface to subsurface runoff. Runoff  
 484 decreases are projected to occur in most seasons over southwest Canada, owing to  
 485 relatively large precipitation declines (Fig. 3, S5).

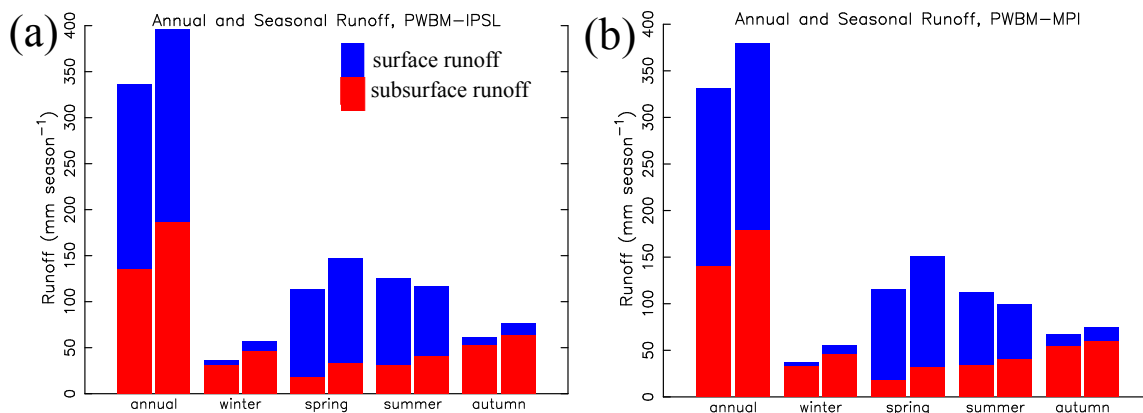


Figure 10: Annual and seasonal total runoff for the early (left bar) and late century (right bar) periods, expressed as surface (blue) and subsurface (red) amounts for (a) PWBm-IPSL and (b) PWBm-MPI simulations.

## 5 Discussion

486 The Arctic basin is drained by several rivers that receive runoff contributions  
 487 over great distances, from grasslands and forests in the south to tundra in the north.  
 488 Surface runoff has typically been a substantial component of river discharge,  
 489 with subsurface flows characterizing low flows in summer and early fall. These character-  
 490 istic patterns and dynamics are shifting due to influences from warming, primarily  
 491 hydrological cycle intensification and permafrost thaw. The shifts are altering the  
 492 water cycle from processes manifesting both horizontally, via primarily atmospheric  
 493 effects, and vertically, from soil thaw, and seasonally, through a combination of both  
 494 impacts. Recent research suggests that a warming Arctic will experience changes in  
 495 moisture sources that will influence freshwater exports from rivers. The two cou-  
 496 pled climate models from which outputs were used in this study capture substantial  
 497 precipitation increases in regions adjacent to the Arctic Ocean. This is a robust  
 498 feature of climate models that is linked to a more open Arctic Ocean later this cen-  
 499 tury (Barnhart et al., 2016; McCrystall et al., 2021). River basins near the western  
 500 Arctic Ocean, particularly far northeast Eurasia, northwest Canada, and northern  
 501 Alaska, will experience relatively large increases in river discharge, driven partly by  
 502 higher snowfall rates and spring SWE amounts. These are cold areas that will warm  
 503 significantly and, in turn, increasingly be fed by additional moisture, including from  
 504 more frequent atmospheric rivers (Zhang et al., 2023). In contrast, southern parts  
 505

506 of the pan-Arctic basin are projected to experience a decline in net precipitation  
507 and runoff contributions to rivers. In general, rivers in central Eurasia and southern  
508 Canada will receive less runoff, particularly during summer. Our results suggest that  
509 nearly 90% of the increase in river discharge from permafrost regions will arise from  
510 an increase in net precipitation (Cubasch et al., 2001), rather than a “de-watering”  
511 of permafrost from thawing soil ice, which likely also played a smaller role over the  
512 20<sup>th</sup> century (McClelland et al., 2004). This connection to net precipitation is con-  
513 sistent with attribution studies for the river discharge trends observed during the  
514 recent past (McClelland et al., 2004, 2006; Zhang et al., 2013). Our results point  
515 to significant shifts in sources of freshwater entering Arctic rivers, with less runoff  
516 to river networks in the south and more in the north. The headwaters of the large  
517 Arctic rivers like the Lena, Ob, Yenisey, Mackenzie, originate well south of what is  
518 typically considered Arctic lands. The simulations suggest that by end of century,  
519 some 20–30% more freshwater discharge will enter, accumulate in, and be export  
520 from the northern half of the four large rivers.

521 In addition to geographic shifts involving atmospheric influences, ongoing soil  
522 thaw and permafrost losses will also influence runoff and materials contributions to  
523 rivers. Our results support a growing body of evidence that deepening active layers  
524 and losses in permafrost extent will increase subsurface runoff contributions to rivers.  
525 Permafrost extent declines by 42 and 63% (PWBM-MPI and PWBM-IPSL respec-  
526 tively) between early (2000–2019) and late (2080–2099) century periods, indicative  
527 of recent and future permafrost degradation. Recent observations in northern Alaska  
528 suggest that increased precipitation and deepening ALT play increasingly important  
529 roles in sustaining low flows and enhancing subsurface hydrologic processes (Arp  
530 et al., 2020; Cooper et al., 2023). Projected changes in subsurface runoff are more  
531 spatially variable compared to total runoff, though a similar south-north gradient  
532 exists. Increased subsurface runoff can lead to decreases in summer stream temper-  
533 atures in headwater catchments (Sjöberg et al., 2021). Pronounced seasonal shifts  
534 in runoff contributions will also occur. Increased runoff in late spring will likely be  
535 driven by higher snow storage and earlier melt that will shift peak spring freshet  
536 runoff earlier by approximately 11 days this century. Increased autumn discharge in  
537 the simulations is not attributable to higher SWE, forced instead by thawing per-  
538 mafrost that is lengthening the period when flow occurs, and creating deeper active  
539 layers that store and release water later in the season. More runoff during November  
540 and December, an approximate 5-fold increase in the modest warming simulation,  
541 highlights the physical connection between warming, permafrost degradation, and  
542 increasing subsurface flows to streams and rivers (St. Jacques and Sauchyn, 2009;  
543 Rawlins et al., 2019). The relatively large changes in November–April runoff de-



544 scribed here are congruent with a recent study that documented a 10% per decade  
545 increase in cold season discharge from nine rivers in Alaska with long data records  
546 (Blaskey et al., 2023). Warming, prominent in this region during autumn and early  
547 winter, can promote increased soil water storage, delaying the release of water into  
548 the streams, and thus contribute to increases in winter flow (Streletskiy et al., 2015).  
549 Results of this study support the hypothesis that across the Arctic basin subsurface  
550 runoff increases will be greatest in permafrost areas.

551 Taken together along with other studies eg. (Mann et al., 2022; Tank et al.,  
552 2023), the spatial shifts suggest alterations in materials exported to coastal waters.  
553 Warming and higher rainfall rates will enhance thaw and increase coastal erosion.  
554 Higher runoff rates will drive additional subsurface contributions of freshwater and  
555 DOC to coastal seas and lagoons (Connolly et al., 2020). More cold season river  
556 discharge has the potential to affect sea ice dynamics and other near-shore processes  
557 involving quantities such as salinity and biogeochemistry. The impacts extend to  
558 water quality and materials exports by rivers. For example, DOC input to the  
559 Arctic Ocean has a very high temporal and geographical variability with a strong bias  
560 towards the large Eurasian Rivers and the freshet period (Amon et al., 2012). Our  
561 results suggest impacts to carbon of differing quality, as Amon et al. (2012) reported  
562 that lignin phenol and p-hydroxybenzene composition of Arctic river DOC point  
563 to the abundance of young, boreal-vegetation-derived leachates during spring flood  
564 and older, soil-, peat-, and wetland-derived DOC during groundwater dominated  
565 low flow conditions. In northern tundra areas where soil carbon amounts are greater,  
566 warmer temperatures and increased runoff will likely lead to increased riverine DOC  
567 exports. Indeed, Frey and Smith (2005) concluded that, assuming no change in  
568 either river discharge or in-channel processes, warming would produce a 2.7–4.4 Tg  
569  $\text{yr}^{-1}$  increase in terrestrial DOC flux from West Siberia to the Arctic Ocean by 2100,  
570 with even larger increases likely should river discharge from the region continue  
571 to increase, as depicted in the simulations examined here. Warming and shifting  
572 snowmelt dynamics could increase transport and mobilization of DOC as subsurface  
573 pathways become active earlier in the year (Croghan et al., 2023). In contrast, some  
574 areas may experience a decrease in DOC export over time due to longer flow paths  
575 and residence times, along with increased microbial mineralization of DOC in the  
576 soil column (Striegl et al., 2005). Increasing soil thaw is expected to accelerate the  
577 release of old carbon (Dean et al., 2018; Schwab et al., 2020), which in turn will be  
578 entrained into, processed by, and exported from Arctic rivers. Moreover, DOC from  
579 deep sediments ( $> 3$  m) could also become a significant contribution of carbon to  
580 Arctic rivers as the climate continues to warm (Mohammed et al., 2022). Nitrate  
581 concentrations are greater at lower latitudes as compared with higher latitudes where

582 permafrost is more prominent (Frey and McClelland, 2009). Changes expressed  
583 predominantly across northern parts of the Arctic basin will have a direct influence  
584 on coastal zone processes. On balance, our results point to continued increases in  
585 DOC export by Arctic rivers, and the mobilization and transport of ancient carbon  
586 in subsurface runoff from permafrost areas.

587 The use of two climate model forcing sets increases confidence in elements of  
588 the model outputs and associated analysis. It is noteworthy that results involving  
589 runoff, in particular the spatial patterns, are similar between the two simulations.  
590 Magnitudes of air temperature and precipitation increases are greater in the sim-  
591 ulation forced with IPSL (PWBM-IPSL). Under those warmer temperatures, the  
592 Hamon potential evapotranspiration function captures the temperature dependence  
593 on actual and potential evapotranspiration. Higher precipitation rates in a warmer  
594 forcing scenario, like IPSL, are offset by higher simulated ET, resulting in relatively  
595 similar magnitudes of annual net precipitation and annual total runoff. This plausi-  
596 ble modeling result suggests less uncertainty with the magnitudes of runoff changes  
597 compared with the changes in meteorological forcings projected by the climate mod-  
598 els. The model validation analysis suggests that the magnitude of simulated annual  
599 total runoff and discharge are comparable to independent observational datasets,  
600 with time trends similar in magnitude to those reported in other studies.

601 Salient conclusions from this study come with caveats related to the limits of  
602 the analysis. Foremost is the large degree of uncertainty in meteorological data  
603 across Arctic regions, attributable to a sparse observation network, as well as un-  
604 certainties in the magnitude of meteorological changes projected by the two coupled  
605 climate models. This uncertainty is ameliorated somewhat through the use of re-  
606 analysis data and model calibration. Results are implicitly linked to the connection  
607 between landscape runoff and river discharge export. Results are also influenced by  
608 the choice of climate model forced under the SSP3-7.0 scenario. In light of this,  
609 one might expect lower magnitudes of change should atmospheric greenhouse gas  
610 concentrations not rise to levels depicted in SSP3-7.0. The broad spatial extent and  
611 moderate model resolution ( $25 \times 25$  km grid cells) employed in this study limit our  
612 ability to incorporate influences such as thermokarst and talik formation on runoff  
613 contributions to streams and rivers. However, it is not clear that these local pro-  
614 cesses are a major component of riverine materials exports by Arctic rivers (Dean  
615 et al., 2018). The model simulations do not include interactions between lakes and  
616 the river networks, so, impacts from lake thaw drainage events (Smith et al., 2005;  
617 Andresen and Lougheed, 2015; Jones et al., 2022) are not simulated. The influence  
618 of land subsidence on soil temperature, moisture, and water storage is also not sim-  
619 ulated. While subsidence is unlikely to lead to abrupt thaw over large areas, it can

620 have significant effects on the hydrology of polygonal tundra, generally increasing  
621 landscape runoff (Painter et al., 2023). The effect on large river basins will depend  
622 on the fraction of those basins that contain polygonal tundra. Our results underscore  
623 the importance in better understanding the myriad transformations reshaping Arctic  
624 environments. Large changes in the far north emphasize the need for more frequent  
625 and spatially extensive sampling of small and medium-sized rivers that ring the Arctic  
626 Ocean. Increased confidence in the magnitude of likely responses will require  
627 a multi-model, multi-scenario ensemble of simulations to obtain a range of projec-  
628 tions consistent with known uncertainties. Incorporating small-scale effects such as  
629 thermokarst and lake drainage on river discharge will require higher-resolution sim-  
630 ulations. New model parameterization obtained from high resolution remote sensing  
631 observations will improve model capabilities in simulating permafrost hydrology in  
632 data sparse regions of the Arctic.

## 633 **6 Code and data availability**

634 The W5E5 data are available at [https://dataservices.gfz-](https://dataservices.gfz-potsdam.de/pik/showshort.php?id=escidoc:4855898)  
635 [potsdam.de/pik/showshort.php?id=escidoc:4855898](https://dataservices.gfz-potsdam.de/pik/showshort.php?id=escidoc:4855898) (last access: 15  
636 October 2022). The MERRA reanalysis data are available at  
637 <https://gmao.gsfc.nasa.gov/reanalysis/MERRA/> (last access: 23 Jan-  
638 uary 2023). The ECMWF Reanalysis v5 (ERA5) data are available at  
639 <https://www.ecmwf.int/en/forecasts/dataset/ecmwf-reanalysis-v5> (last access:  
640 19 March 2023). The TPDC data are available at <http://data.tpdc.ac.cn/en>  
641 (last access: 3 February 2023). The IPA permafrost data in the Circum-  
642 Arctic Map of Permafrost and Ground-Ice Conditions, Version 2 are  
643 available at <https://nsidc.org/data/ggd318/versions/2> (last access 1 Au-  
644 gust 2022). The Global Land Evaporation Amsterdam Model (GLEAM)  
645 data are available at <https://www.gleam.eu/> (last access: 17 April 2023).  
646 The pan-Arctic ET data derived from remote sensing are available at  
647 [http://files.ntsg.umd.edu/data/PA\\_Monthly\\_ET/](http://files.ntsg.umd.edu/data/PA_Monthly_ET/) (last access: 16 April 2023).  
648 Climate model data used as forcings are available in the ISIMIP Repository  
649 located at <https://data.isimip.org/>. Model source code, forcings, parameterizations,  
650 and outputs are available at [https://data.ess-dive.lbl.gov/datasets/ess-dive-](https://data.ess-dive.lbl.gov/datasets/ess-dive-9d7ec367652ba43-20240201T162009168)  
651 [9d7ec367652ba43-20240201T162009168](https://data.ess-dive.lbl.gov/datasets/ess-dive-9d7ec367652ba43-20240201T162009168)

## 652 **7 Author contributions**

653 MAR set up and executed the simulations, analyzed the results, and wrote the  
654 initial draft. AVK prepared the modeling forcing datasets and contributed to the  
655 analysis writing of the accepted manuscript.

## 656 **8 Competing interests**

657 The authors declare that they have no conflict of interest.

## 658 **9 Acknowledgements**

659 The PWBM simulations were performed on high performance computing re-  
660 sources provided by the Massachusetts Green High Performance Computing Center.  
661 We thank John Kimball, James McClelland, Vladimir Alexeev, the two reviewers,  
662 and editor for comments which greatly improved the paper.

## 663 **10 Financial support**

664 This work was supported by funding from the U.S. Department of Energy, Of-  
665 fice of Science, Office of Biological and Environmental Research (Grant No. DE-  
666 SC0019462), the National Aeronautics and Space Administration (Grant No. 80NSSC19K0649),  
667 and the National Science Foundation, Division of Polar Programs (Grant No. NSF-  
668 OPP-1656026).

## 669 **References**

- 670 Ahmed, R., Prowse, T., Dibike, Y., Bonsal, B., and ONeil, H.: Recent Trends in  
671 Freshwater Influx to the Arctic Ocean from Four Major Arctic-Draining Rivers,  
672 *Water*, 12, 1189, <https://doi.org/10.3390/w12041189>, 2020.
- 673 Alexeev, V., Nicolsky, D., Romanovsky, V., and Lawrence, D.: An evaluation of  
674 deep soil configurations in the CLM3 for improved representation of permafrost,  
675 *Geophys. Res. Lett.*, 34, L08501, <http://doi.org/10.1029/2007GL029536>, 2007.
- 676 Amon, R., Rinehart, A., Duan, S., Louchouart, P., Prokushkin, A., Guggenberger,  
677 G., Bauch, D., Stedmon, C., Raymond, P., Holmes, R., et al.: Dissolved organic

- 678 matter sources in large Arctic rivers, *Geochimica et Cosmochimica Acta*, 94, 217–  
679 237, <https://doi.org/10.1016/j.gca.2012.07.015>, 2012.
- 680 Andresen, C. G. and Lougheed, V. L.: Disappearing Arctic tundra ponds:  
681 Fine-scale analysis of surface hydrology in drained thaw lake basins over  
682 a 65 year period (1948–2013), *J. Geophys. Res.-Biogeo*, 120, 466–479,  
683 <https://doi.org/10.1002/2014JG002778>, 2015.
- 684 Anisimov, O. and Reneva, S.: Permafrost and Changing Climate: The Rus-  
685 sian Perspective, *AMBIO: A Journal of the Human Environment*, 35, 169–175,  
686 [https://doi.org/10.1579/0044-7447\(2006\)35\[169:PACCTR\]2.0.CO;2](https://doi.org/10.1579/0044-7447(2006)35[169:PACCTR]2.0.CO;2), 2006.
- 687 Arp, C., Whitman, M., Kemnitz, R., and Stuefer, S.: Evidence of hydrological inten-  
688 sification and regime change from northern Alaskan watershed runoff, *Geophys.*  
689 *Res. Lett.*, 47, e2020GL089186, <https://doi.org/10.1029/2020GL089186>, 2020.
- 690 Arp, C. D. and Whitman, M. S.: Lake basins drive variation in catchment-scale runoff  
691 response over a decade of increasing rainfall in Arctic Alaska, *Hydrol. Process.*,  
692 36, e14583, <https://doi.org/10.1002/hyp.14583>, 2022.
- 693 Barnhart, K. R., Miller, C. R., Overeem, I., and Kay, J. E.: Mapping the  
694 future expansion of Arctic open water, *Nat. Clim. Change.*, 6, 280–285,  
695 <https://doi.org/10.1038/nclimate2848>, 2016.
- 696 Behnke, M. I., McClelland, J. W., Tank, S. E., Kellerman, A. M., Holmes, R. M.,  
697 Haghipour, N., Eglinton, T. I., Raymond, P. A., Suslova, A., Zhulidov, A. V., Gur-  
698 tovaya, T., Zimov, N., Zimov, S., Mutter, E. A., Amos, E., and Spencer, R. G. M.:  
699 Pan-Arctic Riverine Dissolved Organic Matter: Synchronous Molecular Stabili-  
700 ty, Shifting Sources and Subsidies, *Global Biogeochem. Cy.*, 35, e2020GB006871,  
701 <https://doi.org/10.1029/2020GB006871>, 2021.
- 702 Bintanja, R.: The impact of Arctic warming on increased rainfall, *Sci. Rep.*, 8, 1–6,  
703 <https://doi.org/10.1038/s41598-018-34450-3>, 2018.
- 704 Bintanja, R. and Selten, F. M.: Future increases in Arctic precipita-  
705 tion linked to local evaporation and sea-ice retreat, *Nature*, 509, 479482,  
706 <https://doi.org/10.1038/nature13259>, 2014.
- 707 Bintanja, R., van der Wiel, K., Van der Linden, E., Reusen, J., Bogerd,  
708 L., Krikken, F., and Selten, F.: Strong future increases in Arctic precipita-  
709 tion variability linked to poleward moisture transport, *Sci. Adv.*, 6, eaax6869,  
710 <https://doi.org/10.1126/sciadv.aax6869>, 2020.

- 711 Biskaborn, B. K., Smith, S. L., Noetzli, J., Matthes, H., Vieira, G., Strelet-  
712 ski, D. A., Schoeneich, P., Romanovsky, V. E., Lewkowicz, A. G., Abramov,  
713 A., et al.: Permafrost is warming at a global scale, *Nat. Commun.*, 10, 1–11,  
714 <https://doi.org/10.1038/s41467-018-08240-4>, 2019.
- 715 Blaskey, D., Koch, J. C., Gooseff, M. N., Newman, A. J., Cheng, Y., ODon-  
716 nell, J. A., and Musselman, K. N.: Increasing Alaskan river discharge during  
717 the cold season is driven by recent warming, *Environ. Res. Lett.*, 18, 024042,  
718 <https://doi.org/10.1088/1748-9326/acb661>, 2023.
- 719 Box, J. E., Colgan, W. T., Christensen, T. R., Schmidt, N. M., Lund, M., Parmen-  
720 tier, F.-J. W., Brown, R., Bhatt, U. S., Euskirchen, E. S., Romanovsky, V. E.,  
721 et al.: Key indicators of Arctic climate change: 1971–2017, *Environ. Res. Lett.*,  
722 14, 045010, <https://doi.org/10.1088/1748-9326/aafc1b>, 2019.
- 723 Bring, A., Asokan, S. M., Jaramillo, F., Jarsjö, J., Levi, L., Pietroń, J., Prieto,  
724 C., Rogberg, P., and Destouni, G.: Implications of freshwater flux data from the  
725 CMIP5 multimodel output across a set of Northern Hemisphere drainage basins,  
726 *Earth’s Future*, 3, 206–217, <https://doi.org/10.1002/2014EF000296>, 2015.
- 727 Brodzik, M. J. and Knowles, K.: EASE-Grid: A Versatile Set of Equal-Area Pro-  
728 jections and Grids, in M. Goodchild (Ed.) *Discrete Global Grids*. Santa Barbara,  
729 CA, USA: National Center for Geographic Information and Analysis., 2002.
- 730 Brown, J., Jr., O. J. F., Heginbottom, J. A., and Melnikov, E. S.: Circum-Arctic  
731 Map of Permafrost and Ground-Ice Conditions, Tech. rep., National Snow and Ice  
732 Data Center/World Data Center for Glaciology, digital Media, revised 2001, 2001.
- 733 Burke, E. J., Zhang, Y., and Krinner, G.: Evaluating permafrost physics in the  
734 Coupled Model Intercomparison Project 6 (CMIP6) models and their sensitivity  
735 to climate change, *The Cryosphere*, 14, 3155–3174, [https://doi.org/10.5194/tc-14-](https://doi.org/10.5194/tc-14-3155-2020)  
736 [3155-2020](https://doi.org/10.5194/tc-14-3155-2020), 2020.
- 737 Christensen, T. R., Johansson, T., Åkerman, H. J., Mastepanov, M., Malmer, N.,  
738 Friberg, T., Crill, P., and Svensson, B. H.: Thawing sub-arctic permafrost: Ef-  
739 fects on vegetation and methane emissions, *Geophys. Res. Lett.*, 31, L04501,  
740 <https://doi.org/10.1029/2003GL018680>, 2004.
- 741 Clilverd, H. M., White, D. M., Tidwell, A. C., and Rawlins, M. A.: The Sensitivity of  
742 Northern Groundwater Recharge to Climate Change: A Case Study in Northwest

- 743 Alaska, *J. Am. Water Resour. Assoc.*, pp. 1–13, [https://doi.org/10.1111/j.1752-](https://doi.org/10.1111/j.1752-1688.2011.00569.x)  
744 1688.2011.00569.x, 2011.
- 745 Connolly, C. T., Cardenas, M. B., Burkart, G. A., Spencer, R. G., and McClelland, J. W.: Groundwater as a major source of dissolved organic matter to Arctic coastal waters, *Nat. Commun.*, 11, 1–8, [https://doi.org/10.1038/s41467-020-](https://doi.org/10.1038/s41467-020-15250-8)  
746 15250-8, 2020.
- 749 Cooper, M. G., Zhou, T., Bennett, K. E., Bolton, W., Coon, E., Fleming, S. W., Rowland, J. C., and Schwenk, J.: Detecting Permafrost Active Layer Thickness Change From Nonlinear Baseflow Recession, *Water Resour. Res.*, 59, e2022WR033154, <https://doi.org/10.1029/2022WR033154>, 2023.
- 753 Croghan, D., Ala-Aho, P., Lohila, A., Welker, J., Vuorenmaa, J., Kløve, B., Mustonen, K.-R., Aurela, M., and Marttila, H.: Coupling of Water-Carbon Interactions During Snowmelt in an Arctic Finland Catchment, *Water Resour. Res.*, p. e2022WR032892, <https://doi.org/10.1029/2022WR032892>, 2023.
- 757 Cubasch, U., Meehl, G., Boer, G., Stouffer, R., Dix, M., Noda, A., Senior, C., Raper, S., and Yap, K.: Projections of future climate change, chap. , in: JT Houghton, Y. Ding, DJ Griggs, M. Noguer, PJ Van der Linden, X. Dai, K. Maskell, and CA Johnson (eds.): *Climate Change 2001: The Scientific Basis: Contribution of Working Group I to the Third Assessment Report of the Intergovernmental Panel*, pp. 526–582, 2001.
- 763 Cucchi, M., Weedon, G. P., Amici, A., Bellouin, N., Lange, S., Müller Schmied, H., Hersbach, H., and Buontempo, C.: WFDE5: bias-adjusted ERA5 reanalysis data for impact studies, *Earth System Science Data*, 12, 2097–2120, <https://doi.org/10.5194/essd-12-2097-2020>, 2020.
- 767 Dankers, R. and Middelkoop, H.: River discharge and freshwater runoff to the Barents Sea under present and future climate conditions, *Clim. Change*, 87, 131–153, 2008.
- 770 Dean, J., van der Velde, Y., Garnett, M. H., Dinsmore, K. J., Baxter, R., Lessels, J. S., Smith, P., Street, L. E., Subke, J.-A., Tetzlaff, D., et al.: Abundant pre-industrial carbon detected in Canadian Arctic headwaters: implications for the permafrost carbon feedback, *Environ. Res. Lett.*, 13, 034024, <https://doi.org/10.1088/1748-9326/aaa1fe>, 2018.

- 775 Debolskiy, M. V., Alexeev, V. A., Hock, R., Lammers, R. B., Shiklomanov, A.,  
776 Schulla, J., Nicolsky, D., Romanovsky, V. E., and Prusevich, A.: Water balance  
777 response of permafrost-affected watersheds to changes in air temperatures, *Envi-*  
778 *ron. Res. Lett.*, 16, 084 054, <https://doi.org/10.1088/1748-9326/ac12f3>, 2021.
- 779 Del Vecchio, J. D., Palucis, M. C., and Meyer, C. R.: Permafrost extent sets drainage  
780 density in the Arctic, *Proceedings of the National Academy of Sciences*, 121,  
781 e2307072 120, <https://doi.org/10.1073/pnas.2307072120>, 2024.
- 782 Déry, S. J., Hernández-Henríquez, M. A., Burford, J. E., and Wood, E. F.:  
783 Observational evidence of an intensifying hydrological cycle in northern  
784 Canada, *Geophys. Res. Lett.*, 36, <https://doi.org/10.1029/2009GL038852>, L13402,  
785 doi:10.1029/2009GL038852, 2009.
- 786 Du, J., Kimball, J. S., and Jones, L. A.: Passive microwave remote  
787 sensing of soil moisture based on dynamic vegetation scattering prop-  
788 erties for AMSR-E, *IEEE Trans. Geosci. Remote Sens.*, 54, 597–608,  
789 <https://doi.org/10.1109/TGRS.2015.2462758>, 2016.
- 790 Feng, D., Gleason, C. J., Lin, P., Yang, X., Pan, M., and Ishitsuka,  
791 Y.: Recent changes to Arctic river discharge, *Nat. Commun.*, 12, 6917,  
792 <https://doi.org/10.1038/s41467-021-27228-1>, 2021.
- 793 Ford, V. L. and Frauenfeld, O. W.: Arctic precipitation recycling and hydrologic  
794 budget changes in response to sea ice loss, *Global Planet. Change*, 209, 103 752,  
795 <https://doi.org/10.1016/j.gloplacha.2022.103752>, 2022.
- 796 Frey, K. E. and McClelland, J. W.: Impacts of permafrost degradation on arctic river  
797 biogeochemistry, *Hydrol. Process.*, 23, 169–182, <https://doi.org/10.1002/hyp.7196>,  
798 2009.
- 799 Frey, K. E. and Smith, L. C.: Amplified carbon release from vast  
800 West Siberian peatlands by 2100, *Geophys. Res. Lett.*, 32, L09401,  
801 <https://doi.org/10.1029/2004GL022025>, 2005.
- 802 Guo, D., Wang, A., Li, D., and Hua, W.: Simulation of Changes in the Near-Surface  
803 Soil Freeze/Thaw Cycle Using CLM4.5 With Four Atmospheric Forcing Data Sets,  
804 123, 2509–2523, <https://doi.org/10.1002/2017JD028097>, 2018.
- 805 Hinzman, L. D., Deal, C. J., McGuire, A. D., Mernild, S. H., Polyakov, I. V., and  
806 Walsh, J. E.: Trajectory of the Arctic as an integrated system, *Ecol. Appl.*, 23,  
807 1837–1868, <https://doi.org/10.1890/11-1498.1>, 2013.



- 808 Hodson, T. O.: Root-mean-square error (RMSE) or mean absolute error (MAE):  
809 When to use them or not, *Geosci. Model Dev.*, 15, 5481–5487, doi:10.5194/gmd-  
810 15-5481-2022, 2022.
- 811 Hu, Y., Ma, R., Sun, Z., Zheng, Y., Pan, Z., and Zhao, L.: Groundwater Plays an  
812 Important Role in Controlling Riverine Dissolved Organic Matter in a Cold Alpine  
813 Catchment, the QinghaiTibet Plateau, *Water Resour. Res.*, 59, e2022WR032 426,  
814 <https://doi.org/10.1029/2022WR032426>, 2023.
- 815 Hugelius, G., Tarnocai, C., Broll, G., Canadell, J., Kuhry, P., and Swanson, D.: The  
816 Northern Circumpolar Soil Carbon Database: spatially distributed datasets of soil  
817 coverage and soil carbon storage in the northern permafrost regions, *Earth Syst.*  
818 *Sci. Data*, 5, 3–13, <https://doi.org/10.5194/essd-5-3-2013>, 2013.
- 819 Huntington, T. G.: Evidence for intensification of the global water cycle: Review and  
820 synthesis, *J. Hydrol.*, 319, 83–95, <https://doi.org/10.1016/j.jhydrol.2005.07.003>,  
821 2006.
- 822 Huntington, T. G.: Climate Warming-Induced Intensification of the Hydrologic Cy-  
823 cle: An Assessment of the Published Record and Potential Impacts on Agricul-  
824 ture, *Adv. Agron.*, 109, 1–53, [https://doi.org/10.1016/B978-0-12-385040-9.00001-](https://doi.org/10.1016/B978-0-12-385040-9.00001-3)  
825 [3](https://doi.org/10.1016/B978-0-12-385040-9.00001-3), 2010.
- 826 Jin, H., Huang, Y., Bense, V. F., Ma, Q., Marchenko, S. S., Shepelev, V. V., Hu, Y.,  
827 Liang, S., Spektor, V. V., Jin, X., Li, X., and Li, X.: Permafrost Degradation and  
828 Its Hydrogeological Impacts, *Water*, 14, 372, <https://doi.org/10.3390/w14030372>,  
829 2022.
- 830 Jones, B. M., Grosse, G., Farquharson, L. M., Roy-Léveillé, P., Veremeeva, A.,  
831 Kanevskiy, M. Z., Gaglioti, B. V., Breen, A. L., Parsekian, A. D., Ulrich, M.,  
832 et al.: Lake and drained lake basin systems in lowland permafrost regions, *Nat.*  
833 *Rev. Earth Environ*, 3, 85–98, <https://doi.org/10.1038/s43017-021-00238-9>, 2022.
- 834 Koch, J. C., Bogard, M. J., Butman, D. E., Finlay, K., Ebel, B., James, J., John-  
835 ston, S. E., Jorgenson, M. T., Pastick, N. J., Spencer, R. G., et al.: Heterogeneous  
836 Patterns of Aged Organic Carbon Export Driven by Hydrologic Flow Paths, Soil  
837 Texture, Fire, and Thaw in Discontinuous Permafrost Headwaters, *Global Bio-*  
838 *geochem. Cy.*, 36, e2021GB007 242, <https://doi.org/10.1029/2021GB007242>, 2022.
- 839 Koven, C. D., Riley, W. J., and Stern, A.: Analysis of Permafrost Thermal Dynamics  
840 and Response to Climate Change in the CMIP5 Earth System Models, *J. Climate*,  
841 26, 1877–1900, <https://doi.org/10.1175/JCLI-D-12-00228.1>, 2013.

- 842 Lafrenière, M. J. and Lamoureux, S. F.: Effects of changing permafrost condi-  
843 tions on hydrological processes and fluvial fluxes, *Earth-Sci. Rev.*, 191, 212–223,  
844 <https://doi.org/10.1016/j.earscirev.2019.02.018>, 2019.
- 845 Lange, S.: Trend-preserving bias adjustment and statistical downscal-  
846 ing with ISIMIP3BASD (v1. 0), *Geosci. Model Dev.*, 12, 3055–3070,  
847 <https://doi.org/10.5194/gmd-12-3055-2019>, 2019.
- 848 Lange, S.: ISIMIP3BASD, <https://doi.org/10.5281/zenodo.4686991>, 2021.
- 849 Lange, S., Menz, C., Gleixner, S., Cucchi, M., Weedon, G. P., Amici, A., Bel-  
850 louin, N., Schmied, H. M., Hersbach, H., Buontempo, C., and Cagnazzo,  
851 C.: WFDE5 over land merged with ERA5 over the ocean (W5E5 v2.0),  
852 <https://doi.org/10.48364/ISIMIP.342217>, 2021.
- 853 Lawrence, D. M. and Slater, A. G.: Incorporating organic soil into a global climate  
854 model, *Clim. Dynam.*, 30, 145–160, <https://doi.org/10.1007/s00382-007-0278-1>,  
855 2008.
- 856 Liljedahl, A. K., Boike, J., Daanen, R. P., Fedorov, A. N., Frost, G. V., Grosse, G.,  
857 Hinzman, L. D., Iijma, Y., Jorgenson, J. C., Matveyeva, N., et al.: Pan-Arctic ice-  
858 wedge degradation in warming permafrost and its influence on tundra hydrology,  
859 *Nat. Geosci.*, 9, 312–318, <https://doi.org/10.1038/ngeo2674>, 2016.
- 860 Liston, G. E., Haehnel, R. B., Sturm, M., Hiemstra, C. A., Bere-  
861 zovskaya, S., and Tabler, R. D.: Simulating complex snow distribu-  
862 tions in windy environments using SnowTran-3D, *J. Glaciol.*, 53, 241–256,  
863 <https://doi.org/10.3189/172756507782202865>, 2007.
- 864 Liu, S., Wang, P., Yu, J., Wang, T., Cai, H., Huang, Q., Pozdniakov, S. P., Zhang,  
865 Y., and Kazak, E. S.: Mechanisms behind the uneven increases in early, mid-and  
866 late winter streamflow across four Arctic river basins, *J. Hydrol.*, 606, 127425,  
867 <https://doi.org/10.1016/j.jhydrol.2021.127425>, 2022.
- 868 Mann, P. J., Strauss, J., Palmtag, J., Dowdy, K., Ogneva, O., Fuchs, M., Bedington,  
869 M., Torres, R., Polimene, L., Overduin, P., Mollenhauer, G., Grosse, G., Rachold,  
870 V., Sobczak, W., Spencer, R., and Juhls, B.: Degrading permafrost river catch-  
871 ments and their impact on Arctic Ocean nearshore processes, *Ambio*, 51, 439–455,  
872 [doi:10.1007/s13280-021-01666-z](https://doi.org/10.1007/s13280-021-01666-z), 2022.

- 873 Martens, B., Miralles, D. G., Lievens, H., Van Der Schalie, R., De Jeu, R. A.,  
874 Fernández-Prieto, D., Beck, H. E., Dorigo, W. A., and Verhoest, N. E.: GLEAM  
875 v3: satellite-based land evaporation and root-zone soil moisture, *Geosci. Model*  
876 *Dev.*, 10, 1903–1925, <https://doi.org/10.5194/gmd-10-1903-2017>, 2017.
- 877 McClelland, J. W., Holmes, R. M., Peterson, B. J., and Stieglitz, M.: Increasing  
878 river discharge in the Eurasian Arctic: Consideration of dams, permafrost thaw,  
879 and fires as potential agents of change, *J. Geophys. Res.-Atmos.*, 109, D18102,  
880 <https://doi.org/10.1029/2004JD004583>, 2004.
- 881 McClelland, J. W., Déry, S. J., Peterson, B. J., Holmes, R. M., and Wood, E. F.: A  
882 pan-arctic evaluation of changes in river discharge during the latter half of the 20<sup>th</sup>  
883 century, *Geophys. Res. Lett.*, 33, L06715, <https://doi.org/10.1029/2006GL025753>,  
884 2006.
- 885 McCrystall, M. R., Stroeve, J., Serreze, M., Forbes, B. C., and Screen, J. A.: New  
886 climate models reveal faster and larger increases in Arctic precipitation than pre-  
887 viously projected, *Nat. Commun.*, 12, 6765, [https://doi.org/10.1038/s41467-021-](https://doi.org/10.1038/s41467-021-27031-y)  
888 [27031-y](https://doi.org/10.1038/s41467-021-27031-y), 2021.
- 889 McKenzie, J. M., Kurylyk, B. L., Walvoord, M. A., Bense, V. F., Fortier, D., Spence,  
890 C., and Grenier, C.: Invited perspective: What lies beneath a changing Arctic?,  
891 *The Cryosphere*, 15, 479–484, <https://doi.org/10.5194/tc-15-479-2021>, 2021.
- 892 Miralles, D. G., Holmes, T., De Jeu, R., Gash, J., Meesters, A., and Dolman,  
893 A.: Global land-surface evaporation estimated from satellite-based observations,  
894 *Hydrol. Earth Syst. Sci.*, 15, 453–469, <https://doi.org/10.5194/hess-15-453-2011>,  
895 2011.
- 896 Mohammed, A. A., Guimond, J. A., Bense, V. F., Jamieson, R. C., McKenzie, J. M.,  
897 and Kurylyk, B. L.: Mobilization of subsurface carbon pools driven by permafrost  
898 thaw and reactivation of groundwater flow: a virtual experiment, *Environ. Res.*  
899 *Lett.*, 17, 124 036, <https://doi.org/10.1088/1748-9326/aca701>, 2022.
- 900 Nash, D., Waliser, D., Guan, B., Ye, H., and Ralph, F. M.: The Role of Atmospheric  
901 Rivers in Extratropical and Polar Hydroclimate, *J. Geophys. Res.-Atmos.*, 123,  
902 6804–6821, <https://doi.org/10.1029/2017JD028130>, 2018.
- 903 Ni, J., Wu, T., Zhu, X., Hu, G., Zou, D., Wu, X., Li, R., Xie, C., Qiao, Y., Pang,  
904 Q., et al.: Simulation of the Present and Future Projection of Permafrost on the

- 905 Qinghai-Tibet Plateau with Statistical and Machine Learning Models, *J. Geophys.*  
906 *Res.-Atmos.*, 126, e2020JD033402, <https://doi.org/10.1029/2020JD033402>, 2021.
- 907 Nicolsky, D., Romanovsky, V., Alexeev, V., and Lawrence, D.: Improved modeling  
908 of permafrost dynamics in a GCM land-surface scheme, *Geophys. Res. Lett.*, 34,  
909 L08501, <https://doi.org/10.1029/2007GL029525>, 2007.
- 910 Overland, J., Dunlea, E., Box, J. E., Corell, R., Forsius, M., Kattsov, V., Olsen,  
911 M. S., Pawlak, J., Reiersen, L.-O., and Wang, M.: The urgency of Arctic change,  
912 *Polar Sci.*, 21, 6–13, <https://doi.org/10.1016/j.polar.2018.11.008>, 2019.
- 913 Painter, S. L., Coon, E. T., Khattak, A. J., and Jastrow, J. D.: Drying of tundra  
914 landscapes will limit subsidence-induced acceleration of permafrost thaw, *Proc.*  
915 *Natl. Acad. Sci.*, 120, e2212171120, <https://doi.org/10.1073/pnas.2212171120>, 2023.
- 916 Peng, X., Zhang, T., Frauenfeld, O. W., Wang, K., Luo, D., Cao, B., Su, H., Jin, H.,  
917 and Wu, Q.: Spatiotemporal Changes in Active Layer Thickness under Contempo-  
918 rary and Projected Climate in the Northern Hemisphere, *J. Climate*, 31, 251–266,  
919 <https://doi.org/10.1175/JCLI-D-16-0721.1>, 2018.
- 920 Peterson, B. J., Holmes, R. M., McClelland, J. W., Vörösmarty, C. J., Lam-  
921 mers, R. B., Shiklomanov, A. I., Shiklomanov, I. A., and Rahmstorf, S.:  
922 Increasing River Discharge to the Arctic Ocean, *Science*, 298, 2171–2173,  
923 <https://doi.org/10.1126/science.1077445>, 2002.
- 924 Ran, Y., Li, X., Cheng, G., Che, J., Aalto, J., Karjalainen, O., Hjort, J., Luoto, M.,  
925 Jin, H., Obu, J., et al.: New high-resolution estimates of the permafrost thermal  
926 state and hydrothermal conditions over the Northern Hemisphere, *Earth Syst. Sci.*  
927 *Data*, 14, 865–884, <https://doi.org/10.5194/essd-14-865-2022>, 2022.
- 928 Rantanen, M., Karpechko, A. Y., Lipponen, A., Nordling, K., Hyvärinen, O., Ru-  
929 osteenoja, K., Vihma, T., and Laaksonen, A.: The Arctic has warmed nearly  
930 four times faster than the globe since 1979, *Commun. Earth Environ.*, 3, 168,  
931 <https://doi.org/10.1038/s43247-022-00498-3>, 2022.
- 932 Rawlins, M. A.: Increasing freshwater and dissolved organic carbon flows  
933 to Northwest Alaskas Elson lagoon, *Environ. Res. Lett.*, 16, 105014,  
934 <https://doi.org/10.1088/1748-9326/ac2288>, 2021.

- 935 Rawlins, M. A., Lammers, R. B., Frohling, S., Fekete, B. M., and Vörösmarty,  
936 C. J.: Simulating Pan-Arctic Runoff with a Macro-Scale Terrestrial Water Bal-  
937 ance Model, *Hydrol. Process.*, 17, 2521–2539, <https://doi.org/10.1002/hyp.1271>,  
938 2003.
- 939 Rawlins, M. A., Steele, M., Holland, M. M., Adam, J. C., Cherry, J. E.,  
940 Francis, J. A., Groisman, P. Y., Hinzman, L. D., Huntington, T. G., Kane,  
941 D. L., and Coauthors: Analysis of the Arctic System for Freshwater Cy-  
942 cle Intensification: Observations and Expectations, *J. Climate*, 23, 5715–5737,  
943 <https://doi.org/10.1175/2010JCLI3421.1>, 2010.
- 944 Rawlins, M. A., Nicolsky, D. J., McDonald, K. C., and Romanovsky, V. E.: Simulat-  
945 ing soil freeze/thaw dynamics with an improved pan-Arctic water balance model,  
946 *J. Adv. Model. Earth Sys.*, 5, 659–675, <https://doi.org/10.1002/jame.20045>, 2013.
- 947 Rawlins, M. A., Cai, L., Stuefer, S. L., and Nicolsky, D. J.: Changing characteristics  
948 of runoff and freshwater export from watersheds draining northern Alaska, *The*  
949 *Cryosphere*, 13, 3337–3352, <https://doi.org/10.5194/tc-13-3337-2019>, 2019.
- 950 Rawlins, M. A., Connolly, C. T., and McClelland, J. W.: Modeling Terrestrial Dis-  
951 solved Organic Carbon Loading to Western Arctic Rivers, *J. Geophys. Res.-Biogeo*,  
952 126, e2021JG006420, <https://doi.org/10.1029/2021JG006420>, 2021.
- 953 Sazonova, T. S. and Romanovsky, V. E.: A model for regional-scale  
954 estimation of temporal and spatial variability of active layer thickness  
955 and mean annual ground temperatures, *Permafrost Periglac.*, 14, 125–139,  
956 <https://doi.org/10.1002/ppp.449>, 2003.
- 957 Schroeder, R., McDonald, K. C., Zimmerman, R., Podest, E., and Rawlins, M.:  
958 North Eurasian Inundation Mapping with Passive and Active Microwave Remote  
959 Sensing, *Environ. Res. Lett.*, 5, 015003, <https://doi.org/10.1088/1748-9326>, 2010.
- 960 Schwab, M. S., Hilton, R. G., Raymond, P. A., Haghypour, N., Amos, E., Tank, S. E.,  
961 Holmes, R. M., Tipper, E. T., and Eglinton, T. I.: An Abrupt Aging of Dissolved  
962 Organic Carbon in Large Arctic Rivers, *Geophys. Res. Lett.*, 47, e2020GL088823,  
963 <https://doi.org/10.1029/2020GL088823>, 2020.
- 964 Serreze, M. C. and Meier, W. N.: The Arctic’s sea ice cover: trends, variability,  
965 predictability, and comparisons to the Antarctic, *Ann. N. Y. Acad. Sci.*, 1436,  
966 36–53, <https://doi.org/10.1111/nyas.13856>, 2019.

- 967 Shapiro, S. S. and Wilk, M. B.: An analysis of variance test for normality (complete  
968 samples), *Biometrika*, 52, 591–611, <https://doi.org/10.2307/2333709>, 1965.
- 969 Shiklomanov, A. I., Lammers, R. B., Lettenmaier, D. P., Polischuk, Y. M., Savichev,  
970 O. G., Smith, L. C., and Chernokulsky, A. V.: Hydrological Changes: His-  
971 torical Analysis, Contemporary Status, and Future Projections, *Regional En-  
972 vironmental Changes in Siberia and Their Global Consequences*, pp. 111–154,  
973 [https://doi.org/10.1007/978-94-007-4569-8\\_4](https://doi.org/10.1007/978-94-007-4569-8_4), 2013.
- 974 Shiklomanov, I. A. and Shiklomanov, A. I.: Climatic Change and Dynamics of River  
975 Discharge into the Arctic Ocean, *Water Resources*, 30, 593–601, 2003.
- 976 Shiklomanov, I. A., Shiklomanov, A. I., Lammers, R. B., Peterson, B. J., and Vörös-  
977 marty, C. J.: The dynamics of river water inflow to the Arctic Ocean, pp. 281–296,  
978 Kluwer Academic Press, Dordrecht, in *The Freshwater Budget of the Arctic Ocean*,  
979 edited by E.I Lewis, et al., 2000.
- 980 Sjöberg, Y., Jan, A., Painter, S. L., Coon, E. T., Carey, M. P., O’Donnell,  
981 J. A., and Koch, J. C.: Permafrost Promotes Shallow Groundwater Flow  
982 and Warmer Headwater Streams, *Water Resour. Res.*, 57, e2020WR027463,  
983 <https://doi.org/10.1029/2020WR027463>, 2021.
- 984 Slater, A. G. and Lawrence, D. M.: Diagnosing Present and Future Permafrost from  
985 Climate Models, *J. Climate*, 26, 5608–5623, [https://doi.org/10.1175/JCLI-D-12-  
00341.1](https://doi.org/10.1175/JCLI-D-12-<br/>986 00341.1), 2013.
- 987 Smith, L. C., Sheng, Y., MacDonald, G. M., and Hinzman, L. D.: Disappearing  
988 Arctic Lakes, *Science*, 308, p. 1429, <https://doi.org/10.1029/2004JD005518>, 2005.
- 989 Spencer, R. G., Mann, P. J., Dittmar, T., Eglinton, T. I., McIntyre, C.,  
990 Holmes, R. M., Zimov, N., and Stubbins, A.: Detecting the signature  
991 of permafrost thaw in Arctic rivers, *Geophys. Res. Lett.*, 42, 2830–2835,  
992 <https://doi.org/10.1002/2015GL063498>, 2015.
- 993 St. Jacques, J. M. and Sauchyn, D. J.: Increasing winter baseflow and mean annual  
994 streamflow from possible permafrost thawing in the Northwest Territories, Canada,  
995 *Geophys. Res. Lett.*, 36, L01401, <https://doi.org/10.1029/2008GL035822>, 2009.
- 996 Streletskiy, D. A., Tananaev, N. I., Opel, T., Shiklomanov, N. I., Nyland,  
997 K. E., Streletskaya, I. D., Shiklomanov, A. I., et al.: Permafrost hydrology

- 998 in changing climatic conditions: seasonal variability of stable isotope compo-  
999 sition in rivers in discontinuous permafrost, *Environ. Res. Lett.*, 10, 095003,  
1000 <https://doi.org/10.1088/1748-9326/10/9/095003>, 2015.
- 1001 Striegl, R. G., Aiken, G. R., Dornblaser, M. M., Raymond, P. A., and Wick-  
1002 land, K. P.: A decrease in discharge-normalized DOC export by the Yukon  
1003 River during summer through autumn, *Geophys. Res. Lett.*, 32, L21413,  
1004 <https://doi.org/10.1029/2005GL024413>, 2005.
- 1005 Stroeve, J. and Notz, D.: Changing state of Arctic sea ice across all seasons, *Environ.*  
1006 *Res. Lett.*, 13, 103001, <https://doi.org/10.1088/1748-9326/aade56>, 2018.
- 1007 Sturm, M. J., Holmgren, J., and Liston, G. E.: A Seasonal Snow Cover Clas-  
1008 sification System for Local to Global Applications, *J. Climate*, 8, 1261–1283,  
1009 [https://doi.org/10.1175/1520-0442\(1995\)008<1261:ASSCCS>2.0.CO;2](https://doi.org/10.1175/1520-0442(1995)008<1261:ASSCCS>2.0.CO;2), 1995.
- 1010 Tananaev, N., Makarieva, O., and Lebedeva, L.: Trends in annual and extreme flows  
1011 in the Lena River basin, Northern Eurasia, *Geophys. Res. Lett.*, 43, 10,764–10,772,  
1012 <https://doi.org/10.1002/2016GL070796>, 2016.
- 1013 Tananaev, N., Teisserenc, R., and Debolskiy, M.: Permafrost Hydrol-  
1014 ogy Research Domain: Process-Based Adjustment, *Hydrology*, 7, 6,  
1015 <https://doi.org/10.3390/hydrology7010006>, 2020.
- 1016 Tank, S. E., Striegl, R. G., McClelland, J. W., and Kokelj, S. V.: Multi-decadal  
1017 increases in dissolved organic carbon and alkalinity flux from the Macken-  
1018 zie drainage basin to the Arctic Ocean, *Environ. Res. Lett.*, 11, 054015,  
1019 <https://doi.org/10.1088/1748-9326/11/5/054015>, 2016.
- 1020 Tank, S. E., McClelland, J. W., Spencer, R. G., Shiklomanov, A. I., Suslova, A.,  
1021 Moatar, F., Amon, R. M., Cooper, L. W., Elias, G., Gordeev, V. V., Guay, C.,  
1022 Gurtovaya, T. Y., Kosmenko, L. S., Mutter, E. A., Peterson, B. J., Peucker-  
1023 Ehrenbrink, B., Raymond, P. A., Schuster, P. F., Scott, L., Staples, R., Striegl,  
1024 R. G., Tretiakov, M., Zhulidov, A. V., Zimov, N., Zimov, S., and Holmes, R. M.:  
1025 Recent trends in the chemistry of major northern rivers signal widespread Arctic  
1026 change, *Nat. Geosci.*, pp. 1–8, doi:10.1038/s41561-023-01247-7, 2023.
- 1027 Wagner, A., Lohmann, G., and Prange, M.: Arctic river dis-  
1028 charge trends since 7 ka BP, *Global Planet. Change*, 79, 48–60,  
1029 <https://doi.org/10.1016/j.gloplacha.2011.07.006>, 2011.

- 1030 Walsh, J. E., Chapman, W. L., Romanovsky, V., Christensen, J. H., and Stendel,  
1031 M.: Global climate model performance over Alaska and Greenland, *J. Climate*,  
1032 21, 6156–6174, <https://doi.org/10.1175/2008JCLI2163.1>, 2008.
- 1033 Walvoord, M. A. and Kurylyk, B. L.: Hydrologic impacts of thaw-  
1034 ing permafrost—A review, *Vadose Zone J.*, 15, vzj2016.01.0010,  
1035 <https://doi.org/10.2136/vzj2016.01.0010>, 2016.
- 1036 Walvoord, M. A. and Striegl, R. G.: Increased groundwater to stream dis-  
1037 charge from permafrost thawing in the Yukon River basin: Potential impacts  
1038 on lateral export of carbon and nitrogen, *Geophys. Res. Lett.*, 34, L12402,  
1039 <https://doi.org/10.1029/2007GL030216>, 2007.
- 1040 Wang, P., Huang, Q., Pozdniakov, S. P., Liu, S., Ma, N., Wang, T., Zhang, Y., Yu,  
1041 J., Xie, J., Fu, G., et al.: Potential role of permafrost thaw on increasing Siberian  
1042 river discharge, *Environ. Res. Lett.*, 16, 034046, [https://doi.org/10.1088/1748-](https://doi.org/10.1088/1748-9326/abe326)  
1043 [9326/abe326](https://doi.org/10.1088/1748-9326/abe326), 2021.
- 1044 Wang, Y.-R., Hessen, D. O., Samset, B. H., and Stordal, F.: Evaluating global  
1045 and regional land warming trends in the past decades with both MODIS and  
1046 ERA5-Land land surface temperature data, *Remote Sens. Environ.*, 280, 113181,  
1047 <https://doi.org/10.1016/j.rse.2022.113181>, 2022.
- 1048 Warszawski, L., Frieler, K., Huber, V., Piontek, F., Serdeczny, O.,  
1049 and Schewe, J.: The inter-sectoral impact model intercomparison project  
1050 (ISI-MIP): project framework, *Proc. Natl. Acad. Sci.*, 111, 3228–3232,  
1051 <https://doi.org/10.1073/pnas.131233011>, 2014.
- 1052 Willmott, C. J. and Matsuura, K.: Advantages of the mean absolute error (MAE)  
1053 over the root mean square error (RMSE) in assessing average model performance,  
1054 *Clim. Res.*, 30, 79, 2005.
- 1055 Willmott, C. J. and Matsuura, K.: Terrestrial Precipitation: 1900–  
1056 2008 Gridded Monthly Time Series, Version 2.01, available online at:  
1057 <http://climate.geog.udel.edu/simclimate/>, 2009.
- 1058 Woo, M.-K., Kane, D. L., Carey, S. K., and Yang, D.: Progress in per-  
1059 mafrost hydrology in the new millennium, *Permafrost Periglac.*, 19, 237–254,  
1060 <https://doi.org/10.1002/ppp.613>, 2008.



- 1061 Yi, Y., Chen, R. H., Kimball, J. S., Moghaddam, M., Xu, X., Euskirchen, E. S., Das,  
1062 N., and Miller, C. E.: Potential Satellite Monitoring of Surface Organic Soil Prop-  
1063 erties in Arctic Tundra From SMAP, *Water Resour. Res.*, 58, e2021WR030957,  
1064 <https://doi.org/10.1029/2021WR030957>, 2022.
- 1065 Zhang, K., Kimball, J. S., Mu, Q., Jones, L. A., Goetz, S. J., and Running,  
1066 S. W.: Satellite based analysis of northern ET trends and associated changes  
1067 in the regional water balance from 1983 to 2005, *J. Hydrol.*, 379, 92–110,  
1068 <https://doi.org/10.1016/j.jhydrol.2009.09.047>, 2009.
- 1069 Zhang, P., Chen, G., Ting, M., Ruby Leung, L., Guan, B., and Li, L.: More frequent  
1070 atmospheric rivers slow the seasonal recovery of Arctic sea ice, *Nat. Clim. Change.*,  
1071 13, 266–273, <https://doi.org/10.1038/s41558-023-01599-3>, 2023.
- 1072 Zhang, S.-M., Mu, C.-C., Li, Z.-L., Dong, W.-W., Wang, X.-Y., Strelet-  
1073 skaya, I., Grebenets, V., Sokratov, S., Kizyakov, A., and Wu, X.-D.:  
1074 Export of nutrients and suspended solids from major Arctic rivers and  
1075 their response to permafrost degradation, *Adv. Clim. Chang.*, 12, 466–474,  
1076 <https://doi.org/10.1016/j.accre.2021.06.002>, 2021.
- 1077 Zhang, X., He, J., Zhang, J., Polyakov, I., Gerdes, R., Inoue, J., and Wu, P.: En-  
1078 hanced poleward moisture transport and amplified northern high-latitude wetting  
1079 trend, *Nat. Clim. Change.*, 3, 47–51, <https://doi.org/10.1038/nclimate1631>, 2013.

1080  
1081  
1082

*Supplemental Information for*  
**Regime Shifts in Arctic Terrestrial Hydrology Manifested  
From Impacts of Climate Warming**

1083 Michael A. Rawlins<sup>1</sup> and Ambarish V. Karmalkar<sup>2,1</sup>

1084 <sup>1</sup>Department of Earth, Geographic, and Climate Sciences, University of Mas-  
1085 sachusetts, Amherst, MA 01003, USA

1086 <sup>2</sup>Department of Geosciences, University of Rhode Island, Kingston, RI 02881, USA

1087 *Correspondence to:* Michael A. Rawlins (mrawlins@umass.edu)

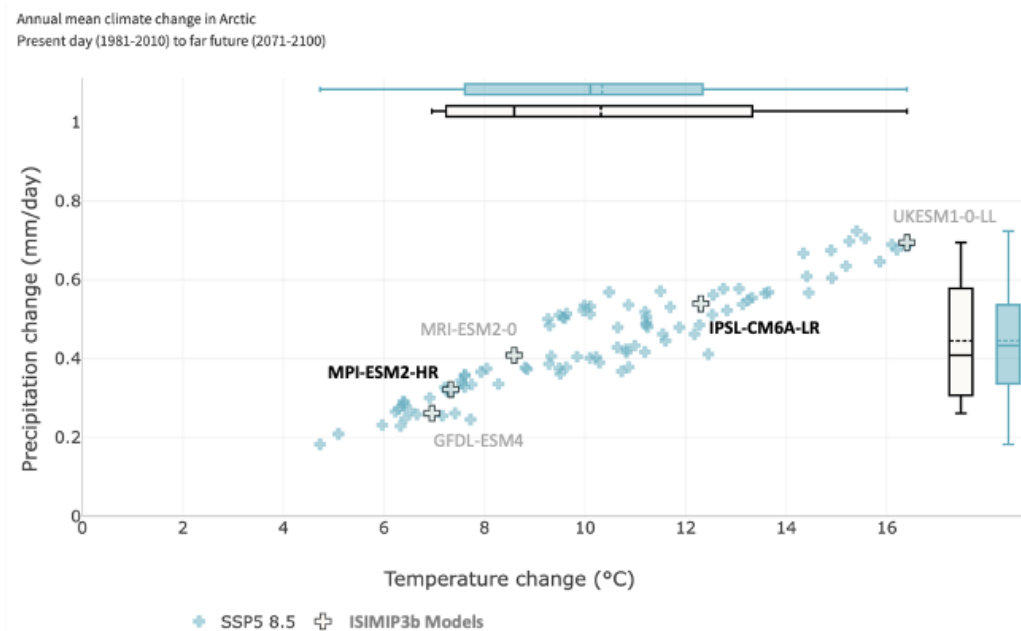


Figure S1: Projected changes in temperature (in °C) and precipitation (in mm day<sup>-1</sup>) for 2070–2100 relative to 1981–2010 mean for the Arctic based on climate models in the CMIP6 archive. The projections are shown for SSP5-8.5. Five CMIP6 models included in ISIMIP3b are highlighted, with the two that were selected as climate inputs in this study shown in bold. Box and whiskers show ranges in temperature and projections spanned by the full CMIP6 ensemble (blue) and the five ISIMIP3b models (black). The figure was created using the GCMeval tool at <https://gcmeval.met.no/>

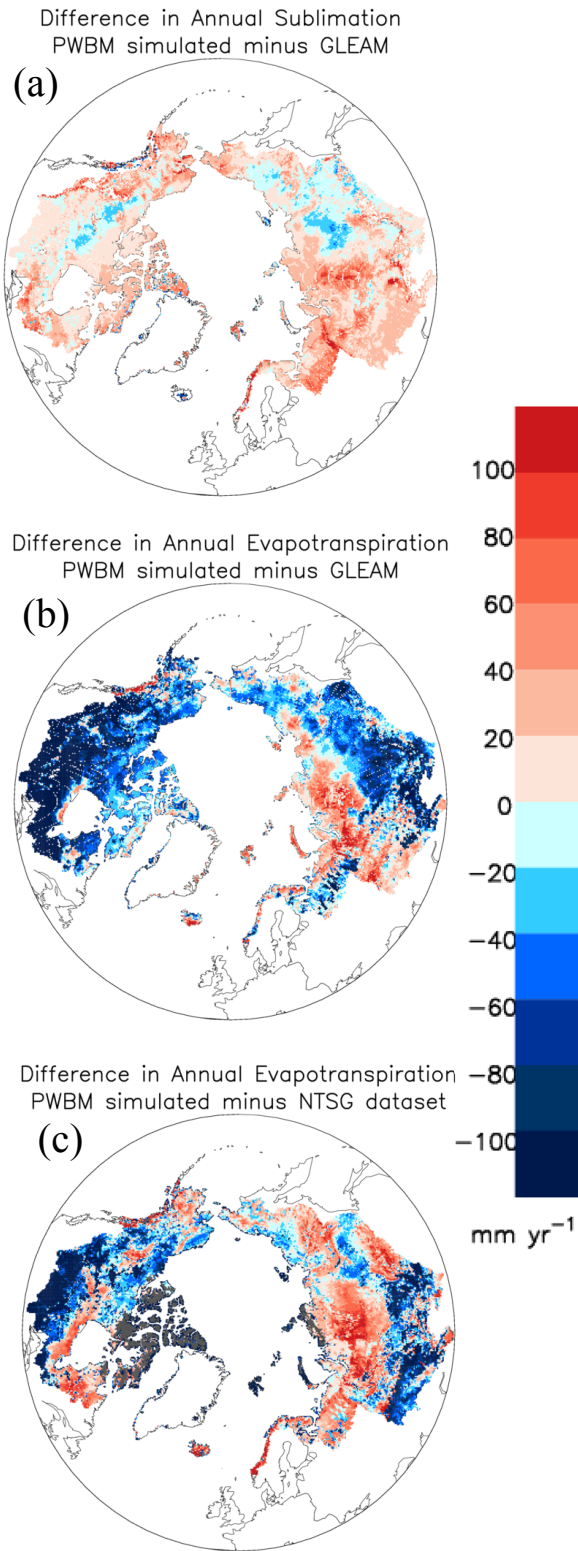


Figure S2: Difference in annual total sublimation ( $\text{mm yr}^{-1}$ ) between simulations with PWBM forced with WFE5 and GLEAM dataset (a) and annual total ET ( $\text{mm yr}^{-1}$ ) between PWBM and GLEAM (b), and difference between PWBM and a dataset made available by the Numerical Terradynamic Simulation Group at the University of Montana (c).

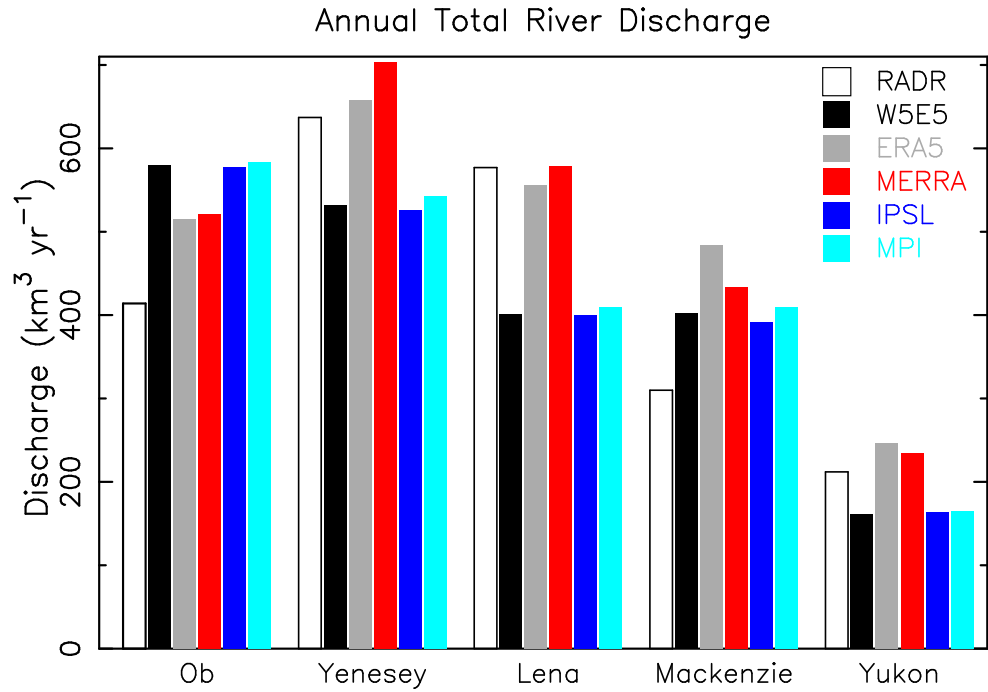


Figure S3: Annual total river discharge ( $\text{km}^3 \text{ yr}^{-1}$ ) for the five largest Arctic rivers. The RADR dataset (Feng et al., 2021) serves as validation for the simulated estimates (PWBM-). Discharge volume shown as an average over the period 1984–2018 for the RADR data, 1980–2019 for the simulations forced by W5E5, ERA5, IPSL, and MPI, and 1980–2013 for the simulation forced by MERRA.

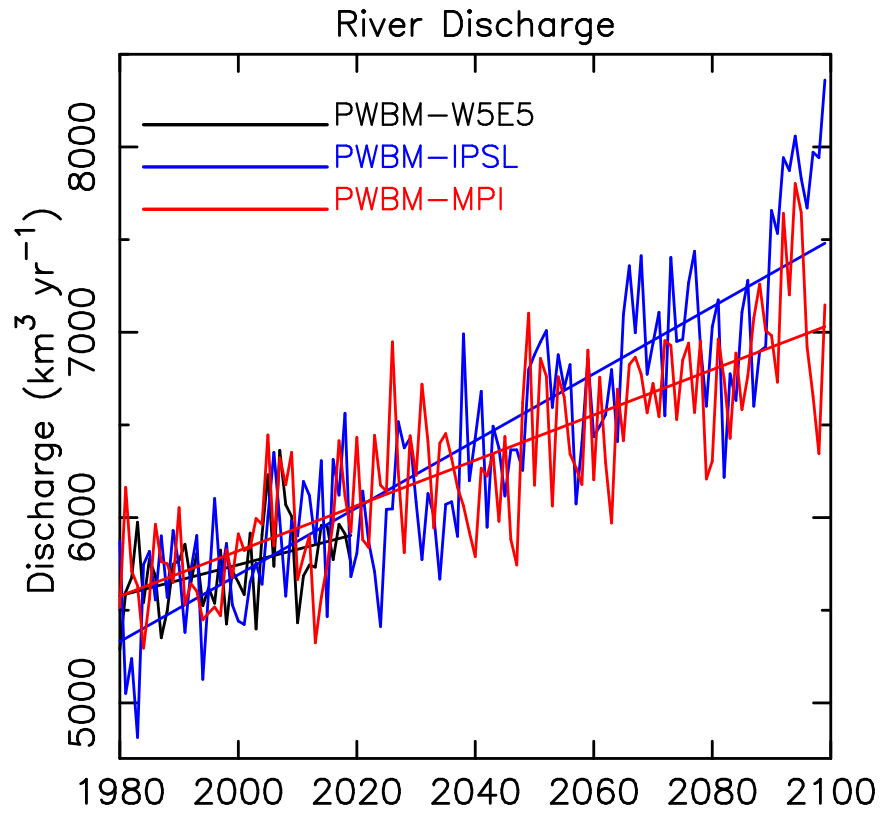


Figure S4: Annual total river discharge (km<sup>3</sup> yr<sup>-1</sup>) from simulations for 1980–2019 and 1980–2100. Linear trend shown.

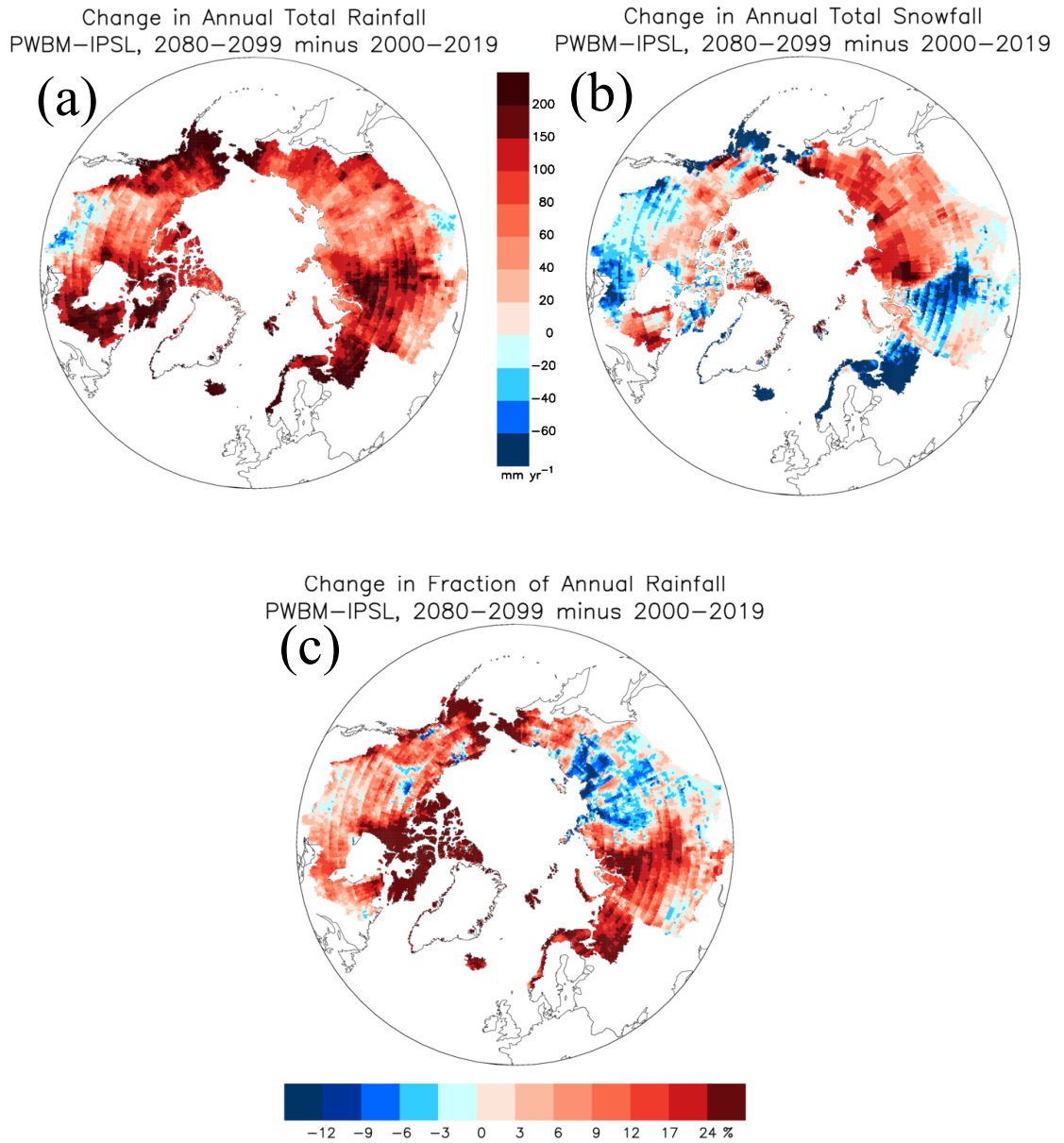


Figure S5: Change in (a) annual rainfall ( $\text{mm yr}^{-1}$ ), (b) snowfall ( $\text{mm yr}^{-1}$ ), and (c) the fraction of rainfall to total precipitation from PWBM-IPSL simulation.

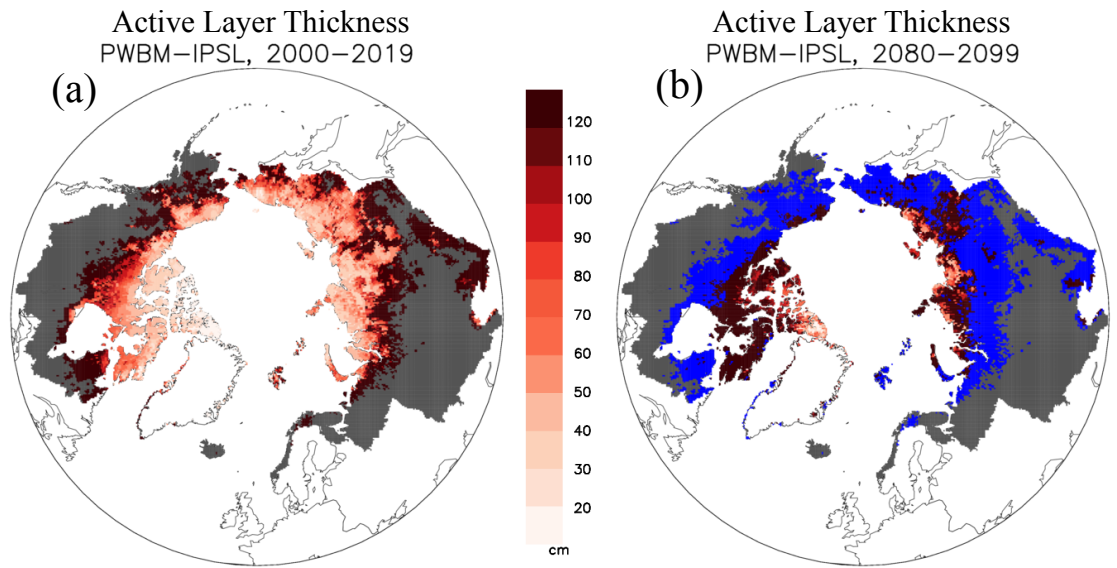


Figure S6: Simulated active-layer thickness (ALT, cm) for (a) early (2000–2019) and (b) late century (2080–2099) periods from PWBM-IPSL. Blue shading highlights areas that are no longer characterized as permafrost in the future period. Gray areas are non-permafrost areas of the Arctic basin.

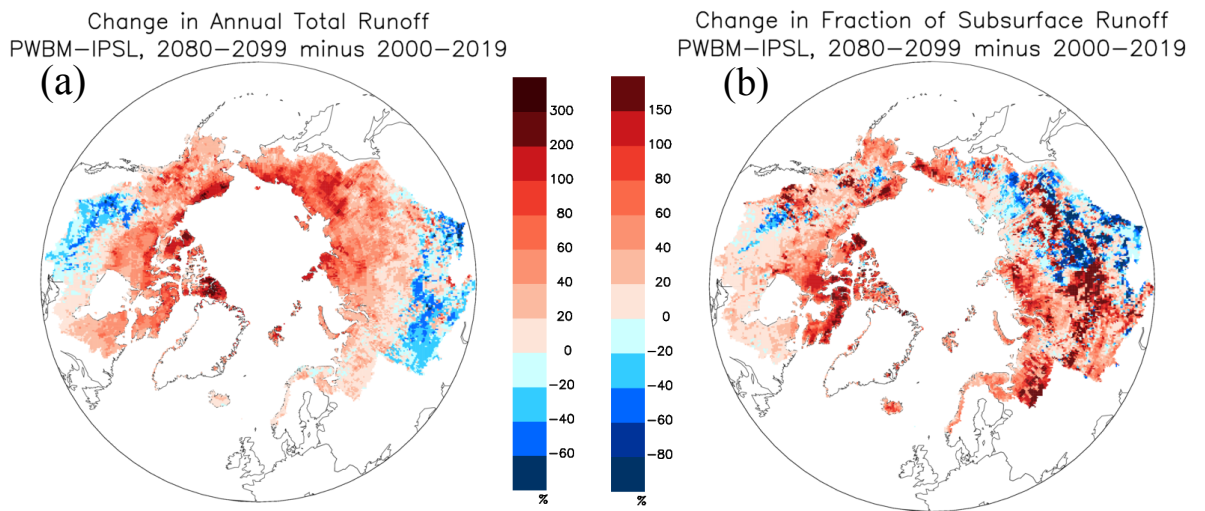


Figure S7: Change in (a) annual total runoff (%) and (b)  $F_{sub}$  (%) from PWBM-IPSL.

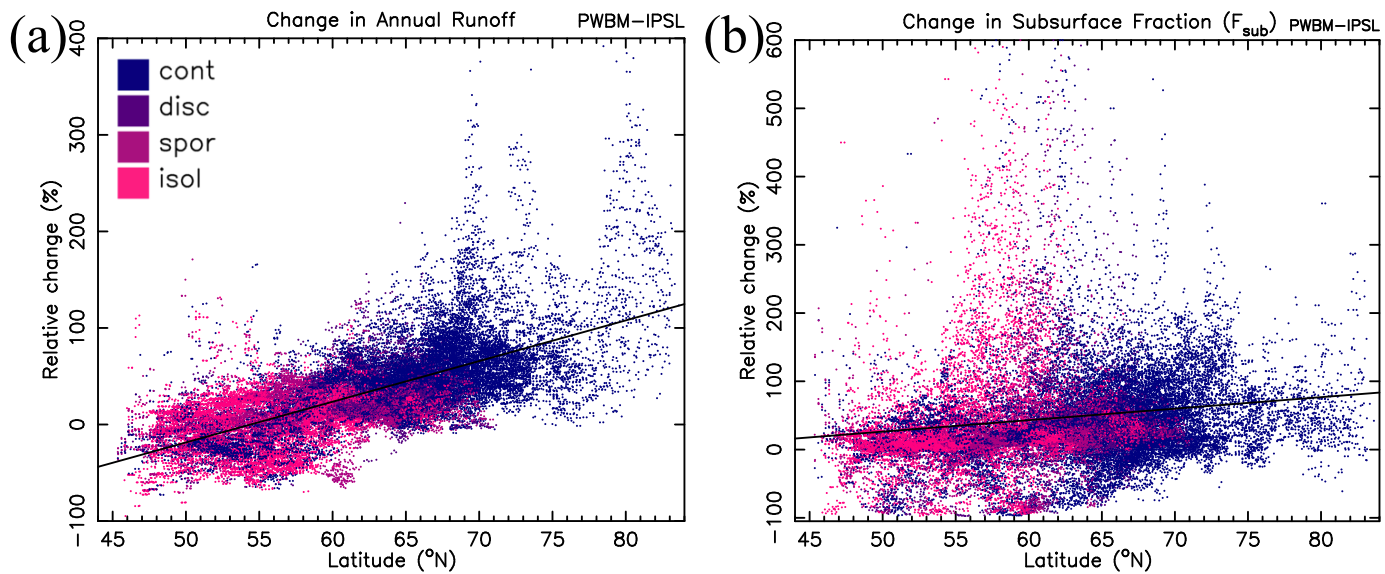


Figure S8: Change in (a) annual total runoff (%) and (b)  $F_{sub}$  with grid cell latitude from PWBM-IPSL simulation for all pan-Arctic domain grid cells. Colors indicate permafrost classification (continuous, discontinuous, sporadic, or isolated) for the cell from IPA dataset (Fig. 1a).

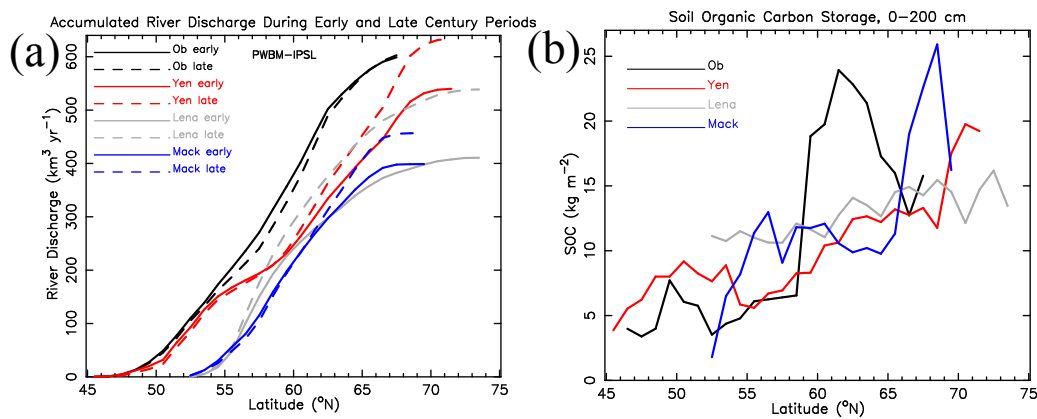


Figure S9: (a) Accumulated annual total river discharge ( $\text{km}^3 \text{yr}^{-1}$ ) for the Ob, Yenese, Lena, and Mackenzie Rivers for  $1^\circ$  latitude bands as averages over early (solid line) and late (dashed) century periods from PWBM-IPSL. (b) Soil carbon storage ( $\text{kg m}^{-2}$ ) in soil 0–200 cm zone from the Northern Circumpolar Soil Carbon Database (Hugelius et al., 2013).



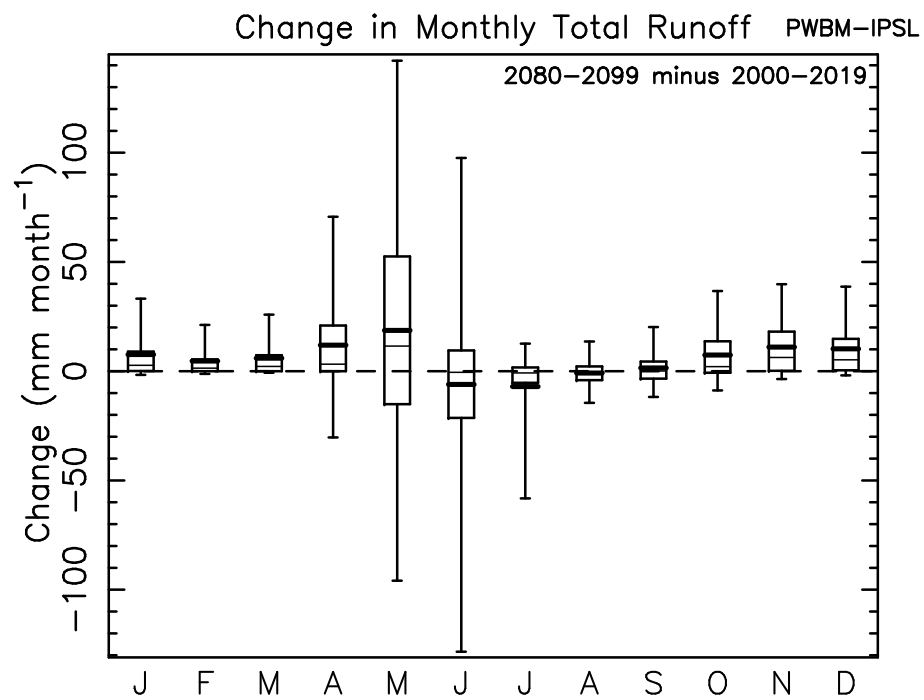


Figure S10: Distribution in change in monthly total runoff (mm month<sup>-1</sup>) between early and late century periods for all pan-Arctic grid cells from PWBM-IPSL.